RESEARCH ARTICLE

ESPL **WILEY**

Alluvial fan response to Alpine Fault earthquakes on the Westland piedmont, Whataroa, Aotearoa-New Zealand

Peter C. Almond[1] | Kelvin Berryman[2] | Pilar Villamor[3] | Stuart Read[3] | Brent V. Alloway[4] | Philip Tonkin[5]

[1]Department of Soil and Physical Sciences, Lincoln University, Christchurch, New Zealand

[2]Berryman Research & Consulting Ltd, formerly GNS Science, Lower Hutt, New Zealand

[3]GNS Science, Lower Hutt, New Zealand

[4]Instituto de Geografía, Pontificia Universidad Católica de Chile, Santiago, Chile

[5]formerly of the Department of Soil and Physical Sciences, Lincoln University, now retired, Christchurch, New Zealand

Correspondence
Peter C. Almond, Department of Soil and Physical Sciences, Lincoln University, Christchurch 7647, New Zealand.
Email: peter.almond@lincoln.ac.nz

Abstract

We examined the stratigraphy of alluvial fans formed at the steep range front of the Southern Alps at Te Taho, on the north bank of the Whataroa River in central West Coast, South Island, New Zealand. The range front coincides with the Alpine Fault, an Australian-Pacific plate boundary fault, which produces regular earthquakes. Our study of range front fans revealed aggradation at 100- to 300-year intervals. Radiocarbon ages and soil residence times (SRTs) estimated by a quantitative profile development index allowed us to elucidate the characteristics of four episodes of aggradation since 1000 CE. We postulate a repeating mode of fan behaviour (fan response cycle [FRC]) linked to earthquake cycles via earthquake-triggered landslides. FRCs are characterised by short response time (aggradation followed by incision) and a long phase when channels are entrenched and fan surfaces are stable (persistence time). Currently, the Te Taho and Whataroa River fans are in the latter phase. The four episodes of fan building we determined from an OxCal sequence model correlate to Alpine Fault earthquakes (or other subsidiary events) and support prior landscape evolution studies indicating ≥M7.5 earthquakes as the main driver of episodic sedimentation. Our findings are consistent with other historic non-earthquake events on the West Coast but indicate faster responses than other earthquake sites in New Zealand and elsewhere where rainfall and stream gradients (the basis for stream power) are lower. Judging from the thickness of fan deposits and the short response times, we conclude that pastoral farming (current land-use) on the fans and probably across much of the Whataroa River fan would be impossible for several decades after a major earthquake. The sustainability of regional tourism and agriculture is at risk, more so because of the vulnerability of the single through road in the region (State Highway 6).

KEYWORDS
aggradation, aggradation and flooding hazard, alluvial fans, Alpine Fault earthquakes, earthquake-triggered landslides, landscape response

1 | INTRODUCTION

Alluvial fans occur in a variety of settings (Blair & McPherson, 2009; Keefer, 1999; Mather et al., 2017) and are sensitive recorders of environmental change and landscape dynamics (Bull, 1977; Field, 2001; Mouchené et al., 2017). The behaviour of alluvial fans is controlled by both allogenic (external) and autogenic (internal) forcing, the effects of which may be difficult to distinguish in their sedimentary archives (Ventra & Nichols, 2014). Autogenic dynamics arise from topographic constraints on sediment accommodation on the fan (causing channel

1804 | wileyonlinelibrary.com/journal/esp

Earth Surf. Process. Landforms. 2023;48:1804–1829.

avulsion) and intrinsic feedbacks between channel gradient and sediment supply (triggering aggradation or incision). Despite these internal dynamics, allogenic controls on net fan building or erosion leave recognisable stratigraphic signatures (Ventra & Nichols, 2014) and have been linked to climate variability (Assine et al., 2014), tectonic activity (DeCelles & Cavazza, 1999), base-level oscillations (Harvey, 2002) or a combination of those factors (Abrams & Chadwick, 1994; Dade & Verdeyen, 2007; Schlunegger & Norton, 2015; Ventra & Nichols, 2014). An allogenic forcing of alluvial fans that has received relatively little attention (Keefer, 1999) is earthquake-triggered landsliding and the effects of the consequent increase in sediment supply (see the review by Fan et al., 2019). The responses to local non-earthquake-triggered landslides provide a general understanding (Davies & Korup, 2007) but do not address the scale, or earthquake magnitude or return-interval dependencies of fan response, and more research is needed in this regard.

The Alpine Fault, bounding the western range front of the Southern Alps in South Island, Aotearoa-New Zealand (Figure 1a), generates regular large to great earthquakes and is late in its earthquake cycle. Alluvial fans formed by large rivers originating at the main divide of the Southern Alps and smaller range front fans draining the Alpine Fault hanging wall are a major geomorphic component of the piedmont at the range front. Nearly all the economic activity, settlements and infrastructure in the region of Westland are on the piedmont. Consequently, understanding the response of these fans to an imminent Alpine Fault earthquake is critical for disaster risk reduction and management.

1.1 | The Alpine Fault

The Alpine Fault is the principal element of the Australia-Pacific plate boundary in the South Island of New Zealand. The fault is generally divided into five sections (Figure 1b) defined by different timings, size and frequency of major (M > 7) to great (M > 8) earthquakes on them (Figure 1c) (Howarth et al., 2018, 2021). The central section of the fault, approximately between Lakes Ellery and Kaniere (Figure 1), spans the parts of Westland where most economic activity, settlements and infrastructure occur. Ruptures on this section have occurred in isolation and in combination with the South Westland section of the fault in great earthquakes that break at least 300 km of the fault between Lake Kaniere and offshore along the Fiordland coast south of John O'Groats River (Figure 1).

The most recent rupture of the central section of the fault in 1717 CE (Howarth et al., 2018; Langridge et al., 2018; Wells et al., 1999) culminated a sequence of paleoearthquakes that occurred at semi-regular intervals of 249 ± 58 years (Howarth et al., 2021), over fault section lengths of 250–400 km, producing large to great earthquakes (Mw ≥ 7.5). There has been no rupture in the time of written record since European colonists arrived in Aotearoa-New Zealand about 1840, but a young event may have occurred on the northern section of the fault in the interval 1813–1848 CE (Langridge et al., 2021). The paleoseismic record indicates that there is a 75% probability of rupture on the central section (single section or multi-section) in the next 50 years (Howarth et al., 2021) and efforts to increase preparedness are underway (Orchiston et al., 2018).
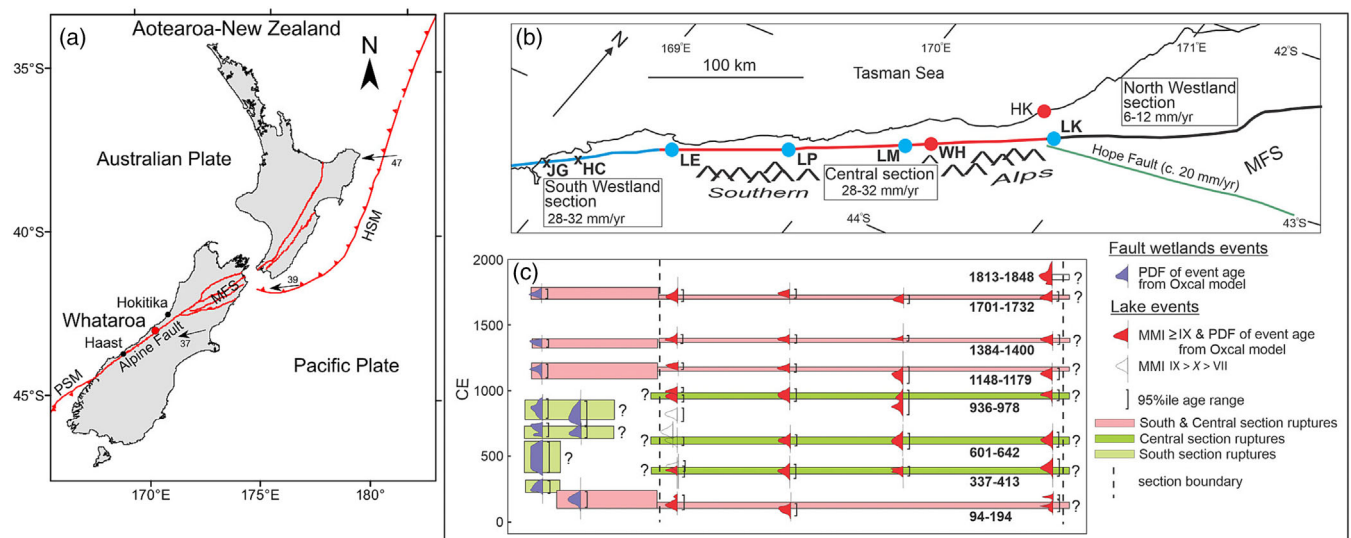

FIGURE 1 Alpine Fault in South Island, New Zealand. (a) Tectonic setting of Aotearoa-New Zealand, including the locations of the Hikurangi Subduction Margin (HSM) in the northeast, the Marlborough Fault System (MFS) and Puysegur Subduction Margin (PSM) in the southwest, and the Alpine Fault. The study area at Whataroa is indicated by a red circle in central Westland. Plate convergence rates (arrows in m ka^{-1}) from DeMets et al. (2010). (b) Fault sections (colour-coded) and average slip rates in each section. Principal locations where paleoseismic data have been obtained—crosses are fault location sites and blue dots are lakes where sedimentary records of earthquakes are preserved. From south to north: JG is John O'Groats River (Cochran et al., 2017); HC is Hokuri Creek (Berryman et al., 2012); LE is Lake Ellery (Howarth et al., 2016); LP is Lake Paringa (Howarth et al., 2014), LM is Lake Mapourika (Howarth et al., 2014); and LK is Lake Kaniere (Howarth et al., 2014; Howarth et al., 2016). Red circles show the location of the study site at Whataroa (WH) and Hokitika (HK) as the principal town of Westland. MFS is the region of the Marlborough Fault System, including the Hope Fault as its southern component. (c) The paleoseismic record showing the timing and likely extent of ruptures on the Alpine Fault in the past 2000 years. Question marks indicate uncertainty in the extent of ruptures across section boundaries. The most recent event (1813–1848 CE) is from fault trenches at the Toaroha River near Lake Kaniere (Langridge et al., 2021). All other events come from Table S6 of Howarth et al. (2021). The extent of this rupture on the North Westland section of the Alpine Fault is unknown. *Source*: Figure modified from Howarth et al. (2021) [Color figure can be viewed at wileyonlinelibrary.com]

The sedimentary record of earthquakes preserved in lake deposits has been particularly important along the central section of the fault. Here, there are few opportunities to trench the fault with much likelihood of being able to date the coarse alluvium typically present in the vicinity of the fault. The most recent reviews of the large earthquake history of the fault, which include the results from lake paleoseismology (Howarth et al., 2018, 2021), indicate the most recent, penultimate and antepenultimate (third to last) events that occurred 1701–1732 CE (most probably 1717 CE based on tree ring studies), 1384–1400 and 1148–1179 CE, respectively. Each of these events appears to have ruptured the southern and central sections of the fault over distances of >300 km in ca. Mw8 earthquakes.

Prior events appear to have sometimes ruptured just the central or southern sections (Figure 1). An important observation from lake record studies is that 40% of all sediment entered the studied lakes in the 50 years following an Alpine Fault event (Howarth et al., 2018).

1.2 | Landsliding and landscape response

Landsliding and aggradation at and west of the range front are recognised as significant, acute and recurrent hazards on account of the possibility of (1) dam-burst floods emanating from landslide dams
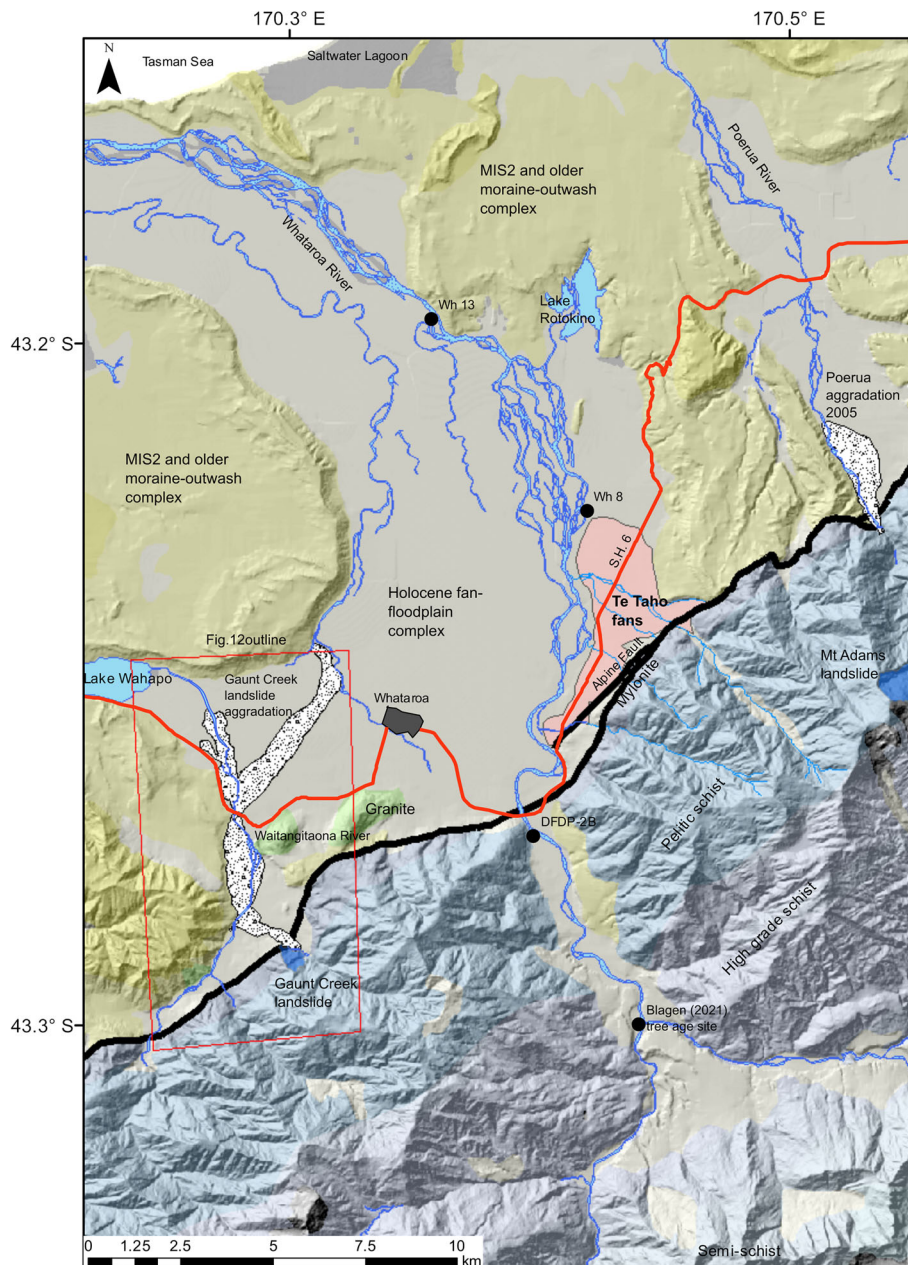

FIGURE 2 Location diagram showing the Te Taho fans along the range front of the Southern Alps adjacent to the Alpine Fault. Background imagery is a hillshade model developed from a 25-m DEM (https://lris.scinfo.org.nz/layer/48127-nzdem-south-island-25-metre/). River polygons from LINZ data service (https://data.linz.govt.nz/layer/50328-nz-river-polygons-topo-150k/). Geology and the delineation of the Alpine Fault trace are from QMap 1:250 000 mapping (Cox & Barrell, 2008). MIS refers to Marine Isotope Stages. The summit of Mt Adams is shown with the location of the 1999 landslide (Korup et al., 2004). Area of Figure 12 is shown as a red rectangle. *Source*: This work includes Toitū Te Whenua Land Information New Zealand data, which are licensed by Toitū Te Whenua Land Information New Zealand for re-use under the Creative Commons Attribution 4.0 International licence [Color figure can be viewed at wileyonlinelibrary.com]

in alpine sections of the river (Robinson & Davies, 2013; Wells & Goff, 2006) and (2) flooding and sedimentation-induced damage to farms and property, and infrastructural lifelines (Orchiston et al., 2018). Most of the understanding of related sediment fluxes is based on (1) decadal landslide inventories in the Southern Alps (Hovius et al., 1997); (2) experience from non-earthquake-related landslides in individual catchments (e.g., Korup, 2005); and (3) volumes of landslide-generated sediment from elsewhere in New Zealand or globally, calibrated against modern sediment loads and an assumption of steady state processes in the Southern Alps where denudation balances mountain building. Current models of landslide generation, sediment flux and hazard for the West Coast invoke an earthquake trigger and have large model uncertainties (Robinson et al., 2016). However, it remains unclear if Alpine Fault and other earthquakes are always the trigger of region-wide landsliding and how well current models capture event-to-event variability in terms of magnitude and locus.

Pre-historic botanical records offer the best potential for assessing the timing and magnitude at a regional scale of past aggradation events on the Westland piedmont. Wells and Goff (2006, 2007) used ages of discrete cohorts of trees on coastal dunes to show that dune formation was episodic and closely tied to Alpine Fault earthquakes. The authors inferred a link between Alpine Fault earthquake-induced landsliding and construction of dunes supplied by longshore drift from river mouths. On fan-floodplain complexes, past recruitment of cohorts of trees into forest stands is compelling evidence of flood or aggradation damage of extant forest. Cullen et al. (2003) evaluated the effect of aggradation and flooding on the Whataroa River fan (Figure 2) in central Westland through analysis of ages of trees in remnant stands of the once ubiquitous rainforest. They showed that forest re-established in two phases corresponding closely to inferred Alpine Fault earthquakes. Moreover, they showed that spatial patterns of regeneration differed, from which they inferred different magnitudes of flooding- or aggradation-related disturbance between the two events. Blagen et al. (2022) expanded on Cullen et al.'s (2003) data set by including tree age data from fan-floodplain complexes north and south of the Whataroa. They concluded similarly that large-scale aggradation was punctuated and consequent on catastrophic landsliding associated with earthquakes on the Alpine Fault or other Southern Alps faults.

1.3 | Purpose

Tree age-based analyses of past aggradation timing and extent are essentially a biologically based surface exposure dating technique. Such studies are limited by (1) the longevity of trees (ca. <1000 years for New Zealand podocarps species); (2) loss of the older part of the disturbance record due to overprint by recent events; and (3) no discrimination between flooding- or aggradation-driven disturbance that initiated establishment of new cohorts of trees. In this paper, we take a single-catchment scale, geological approach to the question of the timing and magnitude of aggradation response to Alpine Fault earthquakes. We consider the stratigraphic record of alluvial fans near Whataroa, which record sedimentation over a period of ~2 ka. We exploit natural exposures in small range front fans, which coalesce and interact with the larger Whataroa River fan. From the stratigraphy and ages of these fans, we interpret fan evolution and the behaviour

of the larger Whataroa fan to which they grade. The stratigraphy, aggradation and soil formation age model we develop provide a basis for (1) considering the link between Alpine Fault earthquakes and alluvial fan sedimentation; (2) quantifying the magnitude and rate of aggradation events; and (3) inferring hazard to infrastructure and economic activity locally and, by extrapolation, to the wider Westland region.

1.4 | The study area

The Whataroa locality in central Westland lies a few kilometres west of the steep range front of the Southern Alps in the central section of the Alpine Fault (Figures 1 and 2). The topographic divide of the Southern Alps parallels the range front about 20 km to the southeast. Between the two lie steep slopes, fissile metamorphic rocks (Alpine Schist) and very high precipitation. From the range front, mean annual rainfall increases from about 5000 mm to reach a peak west of the main divide of about 12 000 mm (Griffiths & McSaveney, 1983). This domain is recognised as having high background erosion rates (Griffiths, 1979; Hovius et al., 1997; Korup, 2005) and efficient fluvial transport of sediment on to the piedmont.

The Whataroa River is the dominant local agent of landscape change on the piedmont. The Whataroa is a large gravel-bed river whose catchment is bounded by the main divide of the Southern Alps in the southeast and covers 453 km^2. The mean annual flow is 134 m^3 s^{-1} generated by a spatially averaged mean annual rainfall of about 8000 mm (Hicks et al., 2011). With a catchment average erosion rate of ~7 mm year^{-1} (Larsen et al., 2014) and a suspended sediment yield estimated to be in the order of 5 Mt year^{-1}, the river delivers more than 5% of the South Island's total suspended sediment budget (Hicks et al., 2011).

At the time of our investigation, the Whataroa River was incised into its fan head (Figure 3) and, at Te Taho on its true right bank, it was carving laterally immediately west of the Alpine Fault. Across the piedmont, the Whataroa River forms an alluvial fan confined by last glacial maximum (32–18 ka) lateral moraines and the Tasman Sea to the northwest (Figure 2). The fan is largely of late Holocene age and represents the upper part of a 400- to 700-m thickness of Quaternary sediment (Davey, 2010). Much of the original podocarp-angiosperm forest of the fan has been cleared in historical times for pastoral farming now comprising a large proportion of intensive dairying.

Our study exploits the exposures of stratigraphy in range front alluvial fans at Te Taho. This setting allows us to quantify landscape evolution in a geomorphic system with large to great earthquakes (Mw ≥ 7.5) occurring at intervals of 200–300 years, a steep range front with slope angles of 30–45° (Figure 3) and annual rainfall of ~5000 mm.

The catchments of the fans we studied are entirely within the amphibolite facies of the Haast Schist on the Alpine Fault hanging wall (Figures 2 and 4). The rocks include abundant pelitic schist (Cox & Barrell, 2008) although mylonitic rocks occur immediately adjacent to the fault (Sibson et al., 1981). Accordingly, the alluvium comprising the fans differs from that of the Whataroa River, which rising close to the Main Divide, is dominated by greywacke lithologies. Thus, the presence or absence of greywacke allowed us to unequivocally distinguish the provenance of coarse clastic sediment in the fans.

FIGURE 3 Photo of Whataroa piedmont looking from the coast towards the Southern Alps. Braided pattern to drainage in foreground is relict from 1717 CE and late 16th or early 17th century fluvial aggradation episodes. *Source*: Photograph courtesy of Graham Hancox, GNS Science [Color figure can be viewed at wileyonlinelibrary.com]
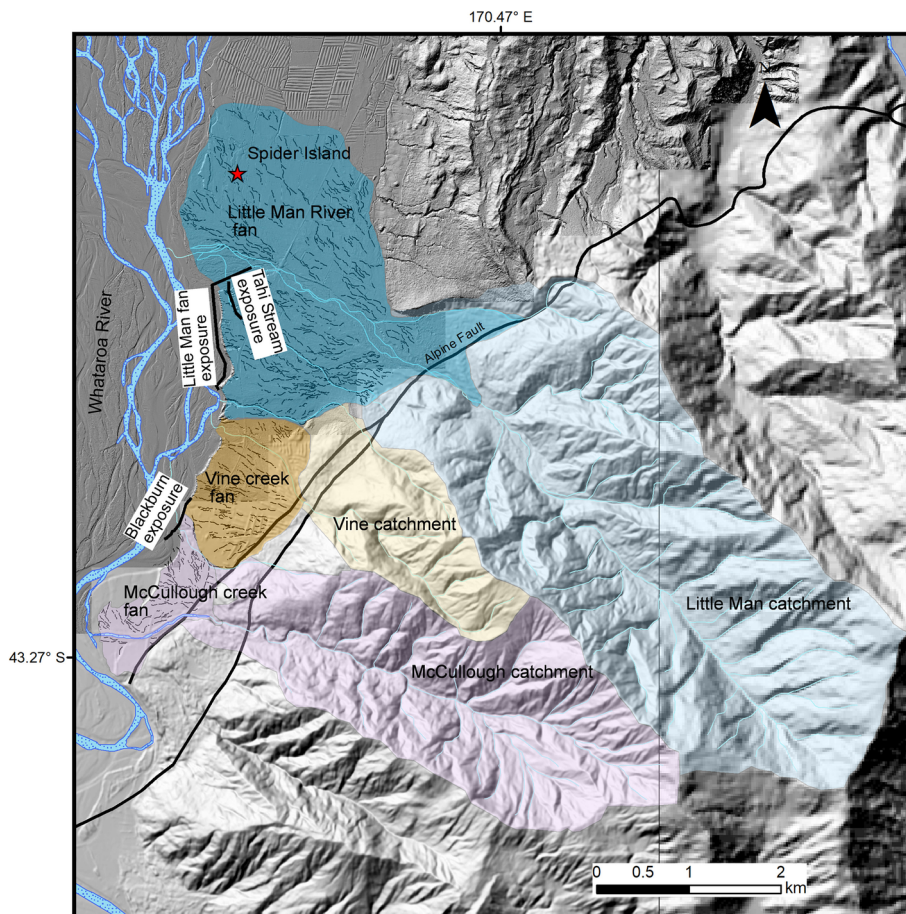

FIGURE 4 Detail of studied fans including their catchments. Relict channel patterns on fan surfaces are delineated with fine lines. Sections sampled and logged in detail are indicated with labelled heavy black lines. Background image is a composite of hillshade based on an 8-m digital surface model developed by photogrammetry (sourced from West Coast Regional Council) and a 25-m DEM (https://lris.scinfo.org.nz/layer/48127-nzdem-south-island-25-metre/). The boundary is delineated with a thin vertical line. The surface traces of the Alpine Fault are shown along the range front. *Source*: This work includes Toitū Te Whenua Land Information New Zealand data, which are licensed by Toitū Te Whenua Land Information New Zealand for re-use under the Creative Commons Attribution 4.0 International licence [Color figure can be viewed at wileyonlinelibrary.com]
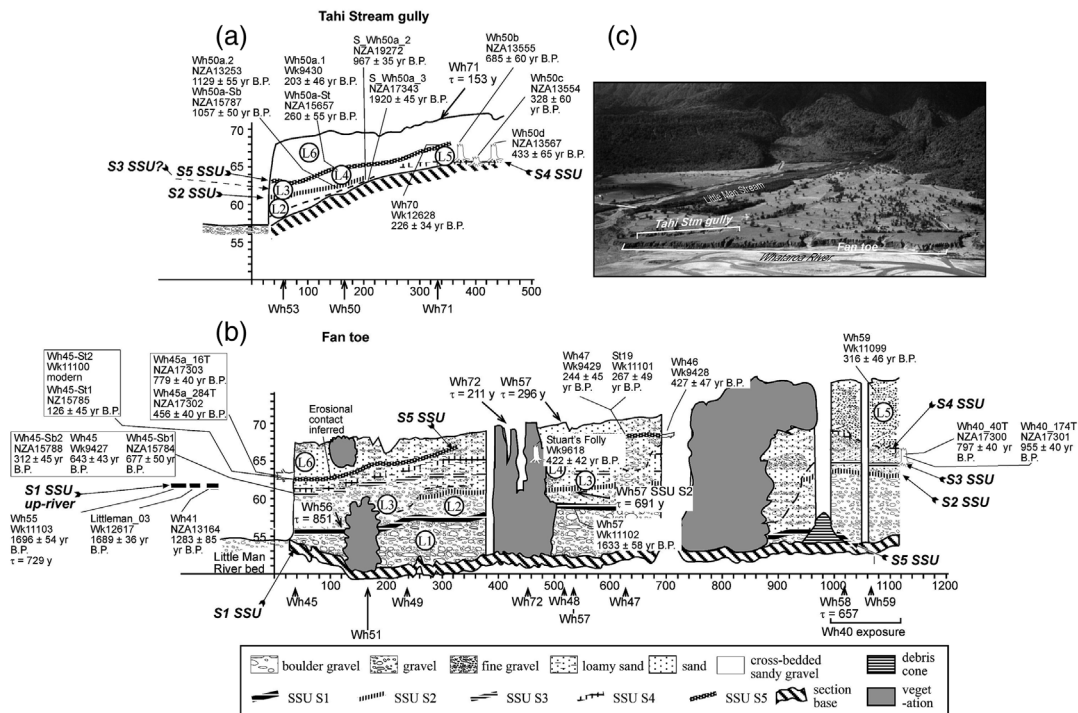
FIGURE 5 Little Man fan stratigraphy and radiocarbon ages along (a) Tahi stream and (b) the fan toe. The nomenclature of sediment packages (L1, L2 etc.), soil stratigraphic units (S1 SSU, S2 SSU etc.) and soil residence times (SRTs) are discussed in the text and Table 1. Section locations and radiocarbon ages are listed in Table S1. The horizontal distance scale is metres southward from the confluence of Little Man River and the Whataroa River, or Tahi stream with Little Man River. Panel (c) shows the location of each on an oblique aerial photograph showing the incised state of the Little Man River from the fan head to the confluence with the Whataroa River, and fan toe erosion by lateral migration of the Whataroa River. The fan toe exposures are approximately 15–20 m high. *Source*: Photograph courtesy of Graham Hancox, GNS Science

Trimming of the toes of the fans by the Whataroa River ('toe-cutting', Leeder & Mack, 2001), incision of streams flowing across the fans and gullies that developed by sapping have exposed the stratigraphy. The streams are entrenched into the fans, both at the fan apex at the range front and where they enter the Whataroa River (Figure 5c), suggesting that the streams have adjusted to limited sediment supply.

The Te Taho fan complex comprises the fans of Little Man River, and Vine and McCullough Creeks. The Little Man fan is a composite fan constructed by Little Man River and three small unnamed streams (Figure 4) draining the Alpine Fault hanging wall. These streams, accordant with their size, likely contribute a small minority of sediment to the fan, but one named informally here Tahi stream is graded to the incised Little Man River and has developed a gully (Tahi gully), which we logged. The combined catchment area contributing to Little Man fan is 15.7 km^2 and the Little Man fan covers 6.78 km^2. Vine and McCulloughs Creeks have catchment areas of 2.98 and 8.03 km^2, and their respective fans cover areas of 1.56 and 0.94 km^2, respectively. For convenience, we name the exposure adjacent to the interfluve between the fans of Vine and McCulloughs Creeks as the Blackburn exposure, after the landholder at the time (2001) (Figure 4). Small, unnamed streams draining the Alpine Fault hanging wall flow into the interfan depression and may have contributed to the fan. Toe-cutting was active in 2001, when data collection for this study started, forming a ~15-m-high N–S-oriented near-vertical scarp then, and continued through to 2021, removing another ~160 m from the toes of the fans. Gully and sapping erosion in response to base level lowering at the fans' toes formed gullies aligned approximately east–west in which there was also semi-continuous exposure.

2 | METHODS

We logged the stratigraphy at selected sites on the fan of Little Man River, and the Blackburn exposure, concentrating on the soil stratigraphy and identification of soil stratigraphic units (SSUs). Our SSUs align in concept with the pedostratigraphic unit of the North American Stratigraphic Code (North American Commission on Stratigraphic Nomenclature, 2005), namely, '… a buried, traceable, three-dimensional body of rock that consists of one or more differentiated pedologic horizons'. Laterally traceable SSUs represent periods when deposition on the fan was minimal. An end to soil formation and death of vegetation growing in a soil occurs at burial, which in the fan context corresponds to the onset of a new aggradation phase. We explore the correlation between fan aggradation and earthquakes sourced from the Alpine Fault or surrounding areas within the Southern Alps after detailing the Te Taho fan stratigraphy and its chronology. SSUs were traced along exposures as visibility permitted and tied together by referencing them to a common vertical datum (mean sea level) with the use of real-time kinematic (RTK) GPS equipment (cm horizontal and vertical accuracy). Nomenclature and description of both soil and sediment followed standard soil description methodologies of Milne et al. (1995) and Schoeneberger et al. (2012).

Organic material from SSUs and intervening sediment packages were collected for radiocarbon dating, with a preference for woody material. Large trees were preserved in association with some SSUs, a few remaining in growth position. From some of these trees, we took samples from two growth rings referenced to ring counts. In this way, we could use Bayesian statistics incorporating age

sequence information to reduce uncertainties on estimates of calibrated radiocarbon ages and estimate the time of tree germination and tree death. When estimating the age of land surface stabilisation using tree germination age, a lag of 23 ± 8 years was added. Here, we assume a normally distributed population of lag times with a mean of 23 years (Wells et al., 1999) and a standard deviation of 8 years. This distribution gives a 95% confidence interval (CI) of 7–39 years, close to the range of germination lags derived by Wells et al. (1999) for podocarps. The Waikato (Wk numbers) or Rafter (NZA numbers) radiocarbon laboratories carried out the analyses. All radiocarbon ages were calibrated against the SHCal20 calibration curve (Hogg et al., 2020) in OxCal (Version 4.4 online, Bronk Ramsey, 2009). We also used increment borers to take cores of living trees to constrain the age of the modern ground surface soil. Tree rings from discs or increment cores were made after sanding to a fine grit. All tree ring counts were assumed to have a ±5% counting error (Wells et al., 1999).

At representative profiles of fine-textured (sandy sediment or finer) surface soil and buried SSUs, we used a corer of 5.4 cm diameter to take soil samples of known volume, which we oven dried and sieved to <2 mm. From these samples, we calculated the bulk density (kg m^{-3}) and then quantified the concentration of secondary pedogenic oxides extractable by acid ammonium oxalate (McKeague & Day, 1966). This reagent extracts poorly crystalline and organically complexed secondary Fe and Al compounds, which are diagnostic of weathering and pedogenesis under the acid leaching regime of the high rainfall West Coast region (Eger et al., 2011; Tonkin & Basher, 1990). The gravimetric oxide concentrations were adjusted to account for Fe and Al extractable at time zero, that is, from unweathered parent material. This baseline value was estimated by analysing the extractable Fe and Al from fresh alluvial sand. After adjustment, gravimetric concentrations were converted to areal masses (kg m^{-2}) by multiplying by the sample increment thickness (m) and the bulk density. We then calculated a profile areal mass of oxalate extractable Fe and Al to the base of a B horizon or 20 cm into the C horizon if no B horizon was present. Thus, the profile aerial mass (PAM) of each analyte is given by

$$PAM_i = \sum_{k=1}^{n} (X_{ik} - X_{ipm}) \rho_{<2\,mm} \cdot h_k, \tag{1}$$

where X_i refers to oxalate extractable Fe or Al concentration. The index k refers to the kth sample of the solum of the (buried) soil, whereas pm refers to the unweathered parent material. A normalised profile development index (PDI) was calculated by dividing the profile aerial masses for each analyte by the corresponding values from a calibration soil of known age, summing and dividing by 2. Thus, the calibration site's PDI evaluated to unity:

$$PDI = \sum_i \frac{\sum_{k=1}^{n} (X_{ik} - X_{ipm}) \rho_{<2\,mm} \cdot h_k}{PAM_{i,ref}} /2. \tag{2}$$

The calibration soil (Wh 65, Figure S1A) came from an isolated remnant of old growth forest on the northern flank of Little Man fan (informally called Spider Island; Figure 4). The site was covered by *Podocarpus totara* forest from which the ages of 19 trees in an even-diameter stand were determined by counting tree rings in cores taken by increment borer in 2001 at 1.5-m height. The soil age was assumed to be the age of the oldest tree plus the germination lag of 23 ± 8 years discussed above. The duration of pedogenesis (soil residence time [SRT], τ) (Yoo & Mudd, 2008) of other soils was estimated by assuming a linear increase of PDI with soil age calibrated against the calibration site:

$$\tau_S = PDI_S \cdot \tau_{ref}, \tag{3}$$

where τ_S, PDI_S and τ_{ref} are the residence time of soil S, the PDI of soil S and the residence time of the soil at the calibration site, respectively. The uncertainty in τ_s was propagated from the uncertainty in age of stabilisation of the surface the tree established on, which determined τ_{ref}.

The chronostratigraphy for each fan was derived using the *Sequence* (italics identify OxCal functions) modelling facility of OxCal. Radiocarbon ages from SSUs were grouped as *Phases* with
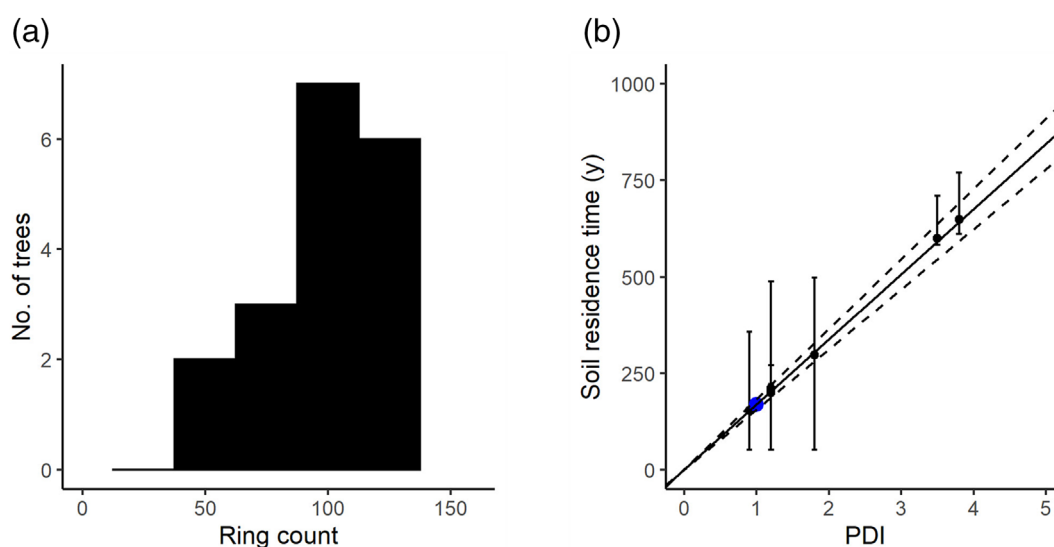
FIGURE 6 Calibration of soil profile development index (PDI): (a) age class distribution of trees on Spider Island; oldest tree 141 years; (b) assumed linear relationship between soil residence time (SRT) (τ) and PDI (see Equation 4) compared against immediately underlying calibrated radiocarbon ages (95% confidence interval). Dashed lines show 95% confidence intervals on the slope of the relationship determined from the 2-sigma uncertainties on the tree establishment time [Color figure can be viewed at wileyonlinelibrary.com]

aggradation (burial) events defined as *Boundaries* stratigraphically above them. SRTs were introduced using the *Before* constraint to require that the burial of SSU_t occurred before burial of $SSU_{t+1} - \tau_{t+1}$. Thus, the age of burial of an SSU minus its SRT established a *Terminus ante quem* for the burial of the immediately underlying SSU. This construction allowed the duration of aggradation to be implicitly determined. Uncertainties in SRTs were determined from the uncertainty in the slope of the PDI versus τ relationship (Figure 6) or from the standard error of the mean (SEM) where more than one estimate of τ from an SSU existed. For trees with more than one radiocarbon dated ring, germination ages, ages of land surface stabilisation and ages of tree death were estimated in distinct *Sequence* models. The models used the *D-sequence* wiggle matching functionality of OxCal to account for radiocarbon ages and ring number *Gaps* between. Outputs were exported as *Priors* that were incorporated back into the appropriate fan chronostratigraphic model. Inter-event intervals were calculated using the *Difference* operator, whereas the duration of aggradation events was calculated as the *Difference* between inter-event interval and the residence time of the SSU formed on the aggradation deposit. Code for all OxCal models is included in the Supporting Information, Text ST3.

3 | RESULTS

3.1 | Little Man fan

3.1.1 | Geomorphology

The stratigraphy of Little Man fan was investigated from the lower reach of Little Man River on its true left bank near the confluence with the Whataroa River and south along the exposed toe of the fan (Figure 5). The exposures increased in height from about 12 m at Little Man River to 20 m at the southern end.

3.1.2 | Stratigraphy

We examined near continuous exposure along the fan toe facing the Whataroa River floodplain and sparse exposures in a gully formed by Tahi stream, as it drains to Little Man River. Incision in this gully had exhumed three trees in growth position. The log of the exposure (Figure 5) begins at an arbitrary origin in the Little Man River bed with elevations of stratigraphic units projected onto a vertical plane with orientation 356°. The section was about 1100 m in length. Two gullies

TABLE 1 Normalised profile development index (PDI) and estimated soil residence time (τ) of surface soils and soil stratigraphic units (SSUs) on the Little Man and Blackburn fans. Also included is the PDI and estimated age of the calibration site at Wh 65 (Spider Island).

Location	Soil stratigraphic unit	Soil profile	Normalised PDI	Soil residence time (years) (±1σ)
Calibration site				
		Wh 65	1.0	169 (36)
Little Man fan				
	Surface soil			
	Tahi gully	Wh 71	0.9	153 (33)
	Fan toe	Wh 57c	1.8	296 (64)
		Wh 72	1.2	211 (46)
	Surface soil mean		1.3	220
	SEM			42
	S4–S2	Wh 53	9.3	1570 (340)
	S2	Wh 57b	4.1	691 (149)
	S1	Wh 55	4.3	729 (157)
		Wh 56	5.0	851 (183)
		Wh 58	3.9	657 (141)
	S1 mean		4.4	746
	SEM			57
Blackburn fan				
	Surface soil			
	Blackburn south	Wh 73	1.2	199 (43)
	Blackburn north	Wh 67	3.2	533 (114)
		Wh 61	3.5	600 (129)
	Blackburn N surface soil mean		3.4	566
	SEM			17
	S4	Wh 61 PS1	1.3	214 (46)
	S3	Wh 61 PS2	1.4	240 (52)
	S2	Wh 61 PS3	7.0	1189 (256)
	S1	Wh 62	7.6	1288 (277)

formed by sapping erosion in response to base level lowering by trimming of the fan toe formed between 690 and 740 m (Gully-700) and between 970 and 1000 m (Gully-1000).

Five buried SSUs were recognised along the fan toe exposure, of which three were also found in Tahi stream. The SSUs are labelled S1–5 from stratigraphically lowermost to uppermost, and the intervening sediment packages are labelled L1–6 in the same stratigraphic order.

3.1.3 | Little Man fan SRTs and chronostratigraphy

SRTs were estimated from their PDI and a linear relationship between PDI and soil age calibrated against the calibration site on Spider Island. The soil there was a Typic Fluvial Recent Soil with a 22-cm-thick silt loam A horizon over a grey, coarse sandy C horizon (Figure S1A). The profile areal masses of Fe_{ox} and Al_{ox} were ~76 and 16 kg m^{-2}, respectively. The 19 trees cored at the site yielded a unimodal age distribution when binned at 25-year age classes with the mode in the range 98–123 years (Figure 6a). The oldest tree had 141 rings, which, allowing for establishment time and ring counting errors, suggests a surface age and SRT of 169 ± 36 years. Assuming a PDI of zero at time zero, Equation (3) evaluates to

$$\tau_S = 169PDI_S. \tag{4}$$

The validity of this relationship was tested against surface soils on both the Little Man fan and Blackburn exposure where local underlying radiocarbon constraint (Figure 6b) existed. Up to SRTs of ca. 600 years, the relationship held well and we extrapolate only to 850 years when determining the residence times of SSUs important for our chronology (Table 1). One would expect the SRT to underestimate the age of burial of the underlying dated material because of the time taken for sediment deposition and any reservoir effect in the buried sample. However, the 2-σ uncertainties on the calibrated radiocarbon ages render any assessment of a systematic difference impossible to evaluate. Equation (4) applied to the PDIs of soils on the Little Man fan produces SRTs varying from 153 to 851 years for simple SSUs, but as high as 1570 years for the cumulate compound soil between S5 and S2 at site Wh 53 (Table 1). In our Bayesian sequence modelling, we used the SEM as a measure of uncertainty of PDI when replicate analyses of an SSU were available; otherwise, we used the uncertainty of the slope of the PDI versus τ relationship (~ ±21% at 1-sigma), which exceeded all SEM values.

Radiocarbon ages from which the chronostratigraphy of the Little Man fan was developed, along with descriptions of SSUs and sediment packages, are presented in Figure 7. Further lithostratigraphic and soil stratigraphic information is provided in the Supporting Information, Text ST1.

We obtained four radiocarbon samples from the S1 SSU, three samples from the banks of Little Man River (samples Wh 41, Wh 55 and Little Man03 in Table S1) and one sample from 540 m along the fan toe exposure (sample Wh 57 in Figure 5 and Table S1). Three of the ages' 95% CIs closely overlapped in the range 251–631 CE (Table S1; see light grey probability density functions [PDFs] in Figure 7). The fourth age had a 95% CI of 654–987 CE. All ages came from roots. The closely aligned ages suggest that this soil was buried

by sediment package L2 at 251–631 CE but that sediment package was locally eroded to allow a later generation of trees (654–987 CE) to exploit the S1 SSU and introduce younger roots. The three sampled soil profiles of the S1 SSU produced a mean residence time of 746 ± 57 years, which when subtracted from the date of that SSU's burial provides a constraint on the end of aggradation of sediment package L1 in which it formed.

Age constraints on the burial of the S2 SSU (formed in sediment package L2) come from Tahi stream gully at or near site Wh 50 where three samples of roots or disseminated organics from within the organic upper horizon gave a range of 773–1207 CE (samples S_Wh 50a_2, Wh 50a-Sb and Wh 50a.2 in Table S1; see light grey PDFs in Figure 7). Fine roots in the S2 SSU from site Wh 53 (Wh 53_Sb in Table S1) at the mouth of Tahi gully gave a spuriously young date of 1636 CE or more recent. The residence time of the S2 SSU (691 years estimated at site Wh 57b) provides for a minimum age constraint on the end of the accumulation of sediment package L2. The latest sediment package L2 could have finished accumulating is 691 years (ignoring uncertainties) before 773–1207 CE, or 82–516 CE. Thus, the minimum age for L2 overlaps with the maximum age (burial of the S1 SSU 251–631 CE), suggesting that the period of aggradation was short.

The timing of burial of the S3 SSU (formed in sediment package L3) by sediment package L4 is established directly from radiocarbon ages at the southern part of the fan toe section. A buried tree at location Wh 40 (Figures 5 and S2) was in growth position and rooted in the S3 SSU. Radiocarbon samples from two sets of rings 134 years apart were dated (rings 39, 40 and 41 and rings 173, 174 and 174, counted from the outside, Table S1). The tree had 196 rings but a rotten centre-most 40 mm. By combining the radiocarbon ages and the tree ring count data in OxCal (Figure S3A) and assuming that accumulation of sediment package L4 killed the tree, the S3 SSU was buried 1230–1344 CE (Figure S3A). The same OxCal model constrains the tree's germination: Accounting for 23 ± 8 years' lag for establishment indicates that aggradation had ceased by 1009–1124 CE. This date range overlaps the timing of burial of the S2 SSU (773–1207 CE) by sediment package L3, in which the S3 SSU forms, suggesting that aggradation of L3 may have been short-lived.

The burial of the S4 SSU by sediment package L5 is dated from the trees in growth position in Tahi stream gully (Wh 50b–d in Table S1; see light grey PDFs in Figure 7) and on the fan toe (Stuart's Folly in Table S1), at 65–66 m ASL. The Stuart's Folly age came from a sample from the rotten outside of a tree (Figure 5) with 178 rings (1445–1628 CE). The trees in Tahi stream were dated from internal rings, two from the centre (Wh 50b with 256 rings and Wh 50d with 140 rings) and one from the 43rd ring from the centre (Wh 50c with 176 rings). Accounting for ring numbers, the ages of burial and death are estimated at 1544–1689, 1564–1779 and 1590–1932 CE, respectively. Together with the tree Stuart's Folly, these ages date burial of the S4 SSU (by L5) at between 1445 and 1932 CE (Table S2). The germination of these trees provides a *terminus ante quem* for the end of accumulation of sediment package L4. The oldest of the minimum ages are the germination of trees Stuart's Folly and Wh 50b at 1235–1419 and 1241–1386 CE, respectively. These dates overlap the timing of burial of the underlying the S3 SSU (1230–1344 CE), which establishes a *terminus post quem* for beginning of accumulation of sediment package L4 (Figure 7). The later germination of the other
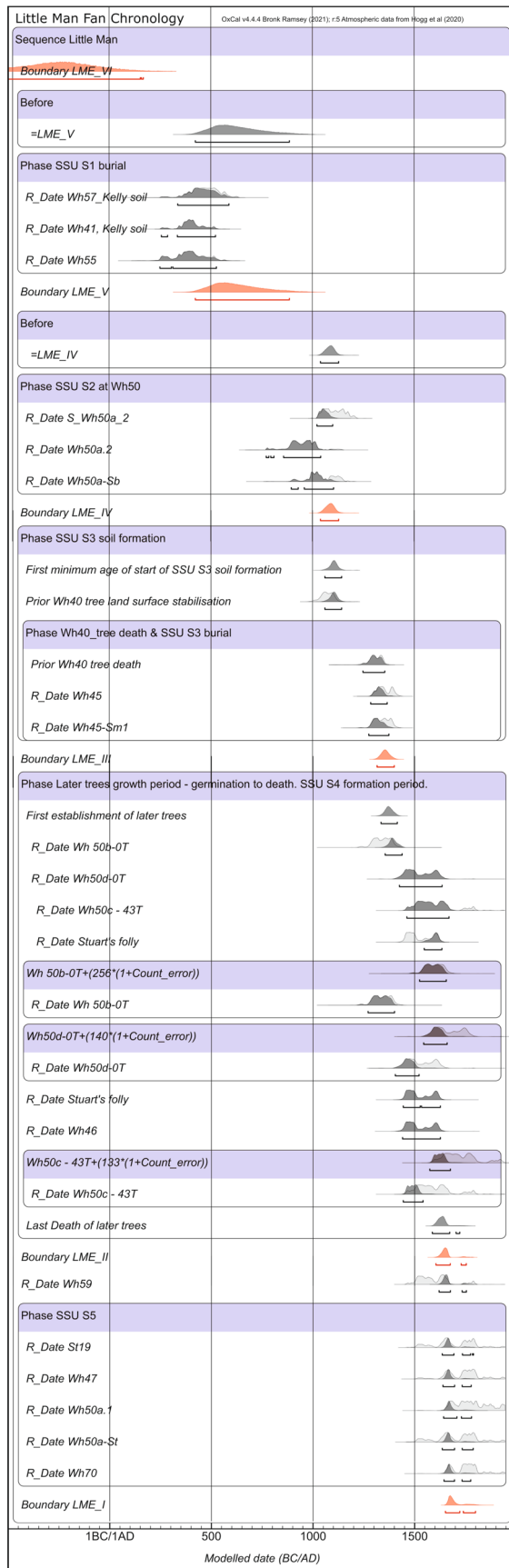
LME_VI
Sediment Package L1. Bouldery to stony gravel up to 6 m thick with a coarse sand matrix comprising sub-round to round schist clasts with weak sub-metre scale bedding.
SSU S1 was an Immature Orthic Brown soil with a 10 – 15 cm – thick loamy silt to sandy loam, dark greyish brown A horizon over a 25-30 cm –thick dark yellowish brown (10YR 4/4), greasy, sandy loam Bs or Bw horizon. PDI = 4.4 +/- 0.3

LME_V burial of SSU S1
Sediment Package L2. 2-9 m of weakly bedded imbricated sandy gravel, to sandy or loamy sediment. Unconformable upper boundary is base of a channel from 880 m to 970 m on the true right of Gully-1000 with layered sands and gravels.
SSU S2. This soil developed in the top of sediment package L2. At the fan toe the soil formed in fine and medium sand with fine gravel stringers, and generally had the morphology of a Weathered Fluvial Recent Soil with an olive brown subsoil (2.5Y 4/2-4). PDI = 4.1

LME_IV burial of SSU S2
Sediment Packages L3 and L4. These sediment packages comprised generally fine (sandy and loamy) horizontal, normally graded beds (cm to dm-scale) with combined thickness of 6 m. The layers intercalated by multiple cumulate and composite soils varying from Recent soils, showing only development of soil fabric, through to Immature Brown soils with rudimentary B horizons. SSU S3 is a prominent buried soil that separates L3 and L4 where it can be found.
SSU S3. Cumulate Immature Orthic Brown Soil. It was difficult to trace over long distances and was only tentatively mapped over much of the exposure. At the southern end of the fan toe exposure (1125 m) a large dead tree in growth position at 65 m ASL (Wh40) defined the top of the S3 SSU. From 880 m north to Little Man River the SSU was an Immature Brown Soil amongst the cumulate soil-sediment packages of L3 and L4. PDI n.d.

LME_III burial of SSU S3
Sediment package L4 - see above

SSU S4. This SSU had a cumulate Weathered Fluvial Recent Soil morphology, and was buried by sediment package L5. At 470 m a tree in growth position ('Stuart's Folly') corresponds with the S4 SSU. In Tahi gully, the S4 SSU was inferred from the position of the root plates of the three exhumed trees (Wh 50 b, c, d) resting in growth position. PDI n.d.

LME_II - burial of SSU S4
Sediment Package L5. Comprised up to 8 m of cross-bedded channel fill sandy schist gravel, horizontally bedded fine sands and loamy sediment with fine gravelly channel fills or gravel sheets.
SSU S5. The uppermost SSU. Varied from an Immature Brown Soil to Recent Gley Soil. Near Little Man River along the fan toe and in Tahi gully the S5 SSU formed into an erosional surface, which we inferred to cross-cut the underlying SSUs. At the northernmost end of the fan toe exposure, a large prone tree (Wh45) lay immediately above this SSU.

LME_I burial of SSU S5
Sediment package L6. Comprised up to 5 m of generally fine-textured (sandy) sediment with thin beds of fine gravel.

Modern surface soil. Typic Fluvial Recent Soils to Weathered Fluvial Recent Soils. The A horizon, often a dark greyish brown (10YR 4/2) silt loam, has probably changed significantly from its condition prior to forest removal and land use change to pastoral farming. PDI = 1.3 +/- 0.2

FIGURE 7 OxCal sequence model for Little Man fan showing prior (light grey) and modelled (dark grey) calibrated 95% confidence interval probability density functions (PDFs) for radiocarbon ages. PDFs of boundaries between phases define aggradation event timings (red). Text provides summary lithological information. See the Supporting Information, Text ST1 for detailed stratigraphic information and Figure 5 for stratigraphy [Color figure can be viewed at wileyonlinelibrary.com]

two trees (Wh 50c,d) suggests that they established in a subsequent phase of recruitment in an existing forest stand.

A maximum age for burial of the S5 SSU and thus the time of arrival of the uppermost sediment package, L6, is provided by a set of radiocarbon ages from wood material in the SSU (Table S1). The calibrated age ranges are wide, spanning the period 1503–1950 CE (see light grey PDFs in Figure 7), because the calibration curve has a shallow slope and is distinctly non-monotonic through this age range. The S5 SSU contains two prone trees, which we radiocarbon dated. At Wh 45 (located at 70-m distance in Figure 5), a large tree in a prone position (Wh 45a in Table S1) with a total of 430 rings yielded radiocarbon ages of 1220–1383 CE 146 rings from the centre and 1421–1624 CE 414 rings from the centre. Combining the radiocarbon ages and ring count information in OxCal afforded a germination date of 1028–1201 CE and death at 1478–1652 CE (Figure S3B). Both ages suggest that the tree has inbuilt age and neither its germination nor death relates to the S5 SSU. The following appear reasonable: It germinated on sediment package L3 at a similar time to the tree Wh 40; it was killed in place by sediment package L4; and it was felled and transported with sediment package L6, which buries the S5 SSU. Another prone and highly rotted tree (Wh 46 in Table S1) occurred immediately above the S5 SSU on the true right of the Gully at 700-m distance in Figure 5 (~68 m ASL) (Figure S4A). The calibrated radiocarbon date of 1441–1629 CE from the outer part of the tree is also out of stratigraphic order and suggests that it was another tree similarly killed by sediment package L4 but snapped later and incorporated into sediment package L6. We excavated the tree and found no root plate (Figure S4B).

A minimum age of burial of the S5 SSU by sediment package L6 is established by the residence times of three observations of the surface soils at Wh 57c (296 years), Wh 72 (211 years) and Wh 71 (153 years). We rejected the short residence time of the soil at Wh 71, presuming that it relates to late activity of Tahi stream where it is located and used an average residence time of 254 ± 43 years based on the other two sites. This SRT constrains the aggradation event burying the S5 SSU to the first half of the 18th century (Figure 7).

To further refine the precision of the ages of events in the chronology of the Little Man fan, we combined all chronological and stratigraphic information including SRTs with full error propagation (radiocarbon, τ, ring count and establishment lag-time uncertainties) into the OxCal sequence model shown in Figure 7 (model agreement index 87.1%; Bronk Ramsey, 1995). Six aggradation events (I–VI, young to old; Table 2) are recognised with a precision (95% CI) ranging from 85 to 463 years for those with bracketing radiocarbon constraint.

The oldest event, Event VI, is dated only by the interval between it and Event V as determined by the residence time of the S1 SSU and it has low precision (range = 1036 years) (Table 2). Using the more precise dates, there have been five aggradation events in the last ca. 1600 years. The intervals between those events range from <129 to 666 years. Event VI (867 BCE to 169 CE) produced a bouldery and cobbly gravel of indeterminate thickness because its base lies below river bed level, but it appeared almost ubiquitously along-section. Event V (425–888 CE; burying the S1 SSU) produced a dominantly cobbly gravel along the whole section (sediment package L2). Event IV (1041–1130 CE, burying the S2 SSU) was dominantly gravelly near Little Man River but progressively became finer (sand to loamy sand) and thinner away from the fan axis (sediment package L3), suggesting that aggradation was localised to an alluvial ridge located axially as is

the present stream. Event III (1318–1403 CE; burying the S3 SSU) was thin and fine in texture (sandy and fine gravel—sediment package L4), suggesting unconfined sedimentation in the form of levees or crevasse splays (sheetform deposits, Mather et al., 2017). Event II (1605–1754 CE; burying the S4 SSU) produced thick cross-bedded gravels and sands (sediment package L5) on the southern flank of the Little Man fan, suggesting that the stream had avulsed as a result of aggradation. The most recent event (Event I; 1652–1800 CE) burying the S1 SSU was generally fine (sand to sandy fine gravels, sediment package L6) and did not extend to the higher elevations of the southern part of the fan (Figure 5). The behaviour of the Little Man fan over the last ca. 2.5 ka is summarised in Figure 8a.

3.2 | Blackburn exposure

3.2.1 | Geomorphology

The exposures we mapped at the toe of the Blackburn exposure are divided into a north (0–260 m along-section) and a south (330–580 m along-section) section either side of the gully referred to informally as Sheet Creek gully (Figure 9). The exposed section is approximately 750 m south of the junction of Vine Creek and the Whataroa River and there is a gap of approximately 1.3 km with the southern-most exposure of the Little Man fan (Figure 4). At the toe of the Blackburn exposure, a section about 12 m high with fan surface elevations (ASL) ranging from about 75 m in the north to 82 m in the south was mapped. The stratigraphy and location of radiocarbon samples are mapped onto a vertical plane with orientation 036° with an arbitrary origin at the north of the section. Many short and steep sapping-related gullies occurred along the north section. Three of the larger ones, Gley gully at about 60-m distance and Meatloaf gully at about 100-m distance and Sheet Creek (260–330 m), exposed stratigraphy and organic material that was dated. The floodplain of the Whataroa River rose by about 5 m along the fan face, slightly less than the rise of the fan surface, consistent with the location of axis of the McCullough fan further to the south.

3.2.2 | Stratigraphy

Five buried SSUs were recognised along the fan toe exposure. The SSUs are labelled S1–5 from stratigraphically lowermost to uppermost, and the intervening sediment packages are labelled L1–5 (L2 is a composite unit with S2 within the sediment package on the north exposure) (Figures 9 and 10).

3.2.3 | Blackburn exposure SRTs and chronostratigraphy

Radiocarbon ages from which the chronostratigraphy of the Blackburn exposure was developed, along with descriptions of SSUs and sediment packages, are presented in Figure 11. Two radiocarbon ages, both from organic (peaty) silts in the surface of the S1 SSU, one from the south section at 430-m distance (Wh 27) and the other from the north section at 100-m distance (Wh 61; Pal4), yielded non-

TABLE 2 Aggradation event timings, intervals between events, duration of aggradation events (95% CI) and minimum aggradation rates based on OxCal sequence modelling for Little Man fan and Blackburn exposure.

Event	Event timing (CE) From	To	Event horizon elev. (m ASL)	Interval (years) From	To	Duration of aggradation (95% CI bounds) Lower	Upper	Min. agg. rates (mm year⁻¹)	Event timing (CE) From	To	Event horizon elev. (m ASL)	Interval (years) From	To	Duration of aggradation (95% CI bounds) From	To	Min. agg. rates (mm year⁻¹)
	Little Man fan								Blackburn exposure							
2001 CE			71								76					
				200	348							232	409			
I	1652	1800	69			−1	140	14	1589	1768				2	276	
				−2	129							182	398			
II	1605	1754	65						1335	1445	73			−3	96	31
				224	411							205	385			
III	1318	1403	64			−31	154	10	1030	1165				27	207	
				211	335											
IV	1041	1130	62			15	141	11								
				199	666											
V	425	888	59			−2	201	15								
				625	1423											
VI	−867	169														

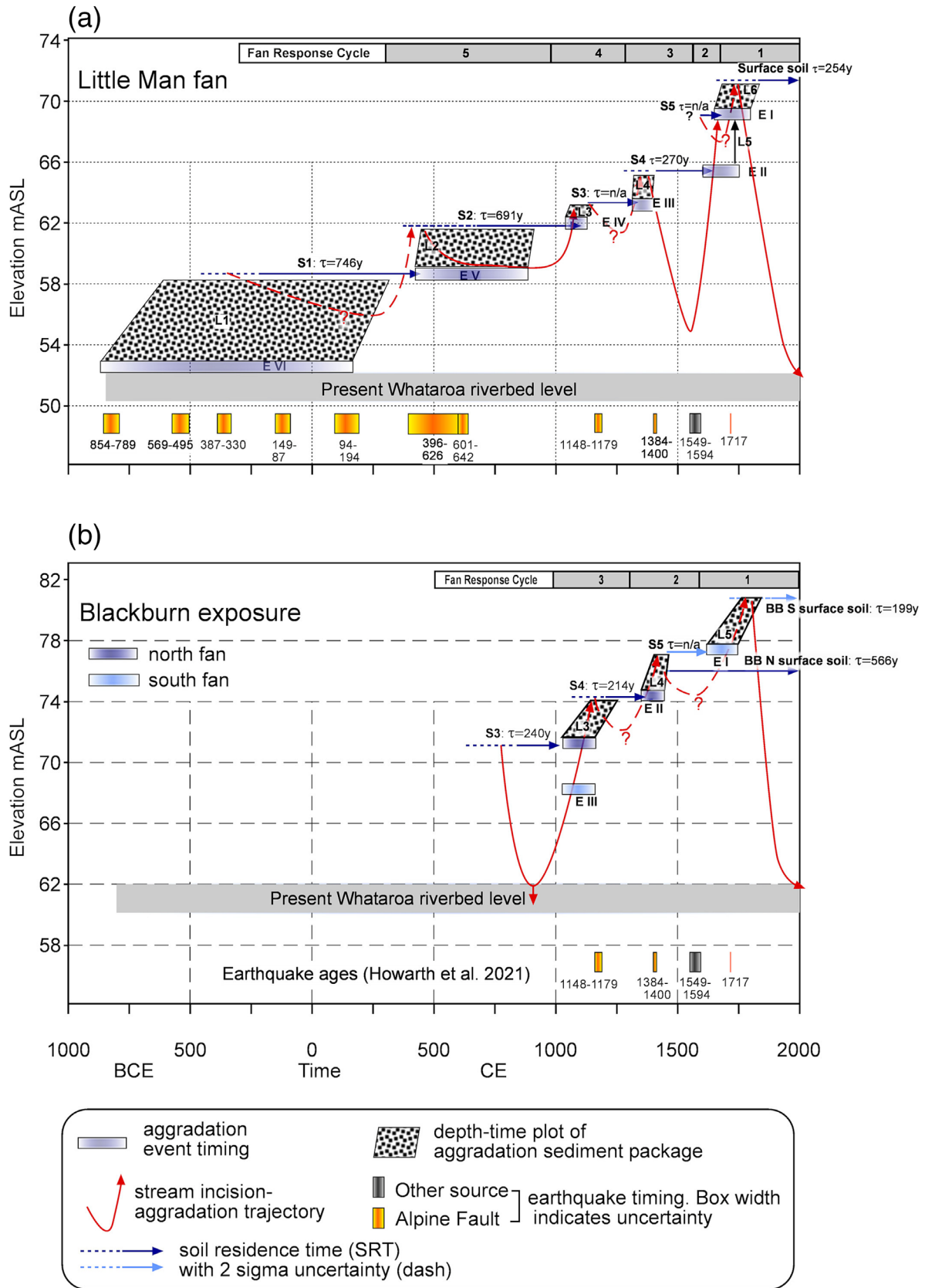Abbreviation: CI, confidence interval.

FIGURE 8 Synthesis of all data pertaining to the evolution of (a) the Little Man fan and (b) the Blackburn exposure for the past ~3 ka. Data include event timing and duration of aggradation based on OxCal models (Table 2 and Figures 7 and 11) of all radiocarbon ages (Table S1), soil residence times (Table 1), correlation with the most recent compilation of timing of Alpine Fault (yellow boxes) and a presumed Southern Alps earthquake (grey box). Event ages have age ranges (horizontal blue bars). Aggradation depth-time is shown by stippled polygons. Soil residence time (τ) as given has quantified or assumed uncertainties in the order of 21%. No data on the SRT for S3 SSU or S5 SSU are available. Incision-aggradation trajectories are drawn so that incision begins contemporaneously with the beginning of pedogenesis (with uncertainty) of SSUs as indicated by SRTs. The subsequent aggradation trajectory is drawn so that pedogenesis of an SSU is curtailed by burial due to the aggradation. Dashed trajectories imply uncertainty on the depth of incision [Color figure can be viewed at wileyonlinelibrary.com]
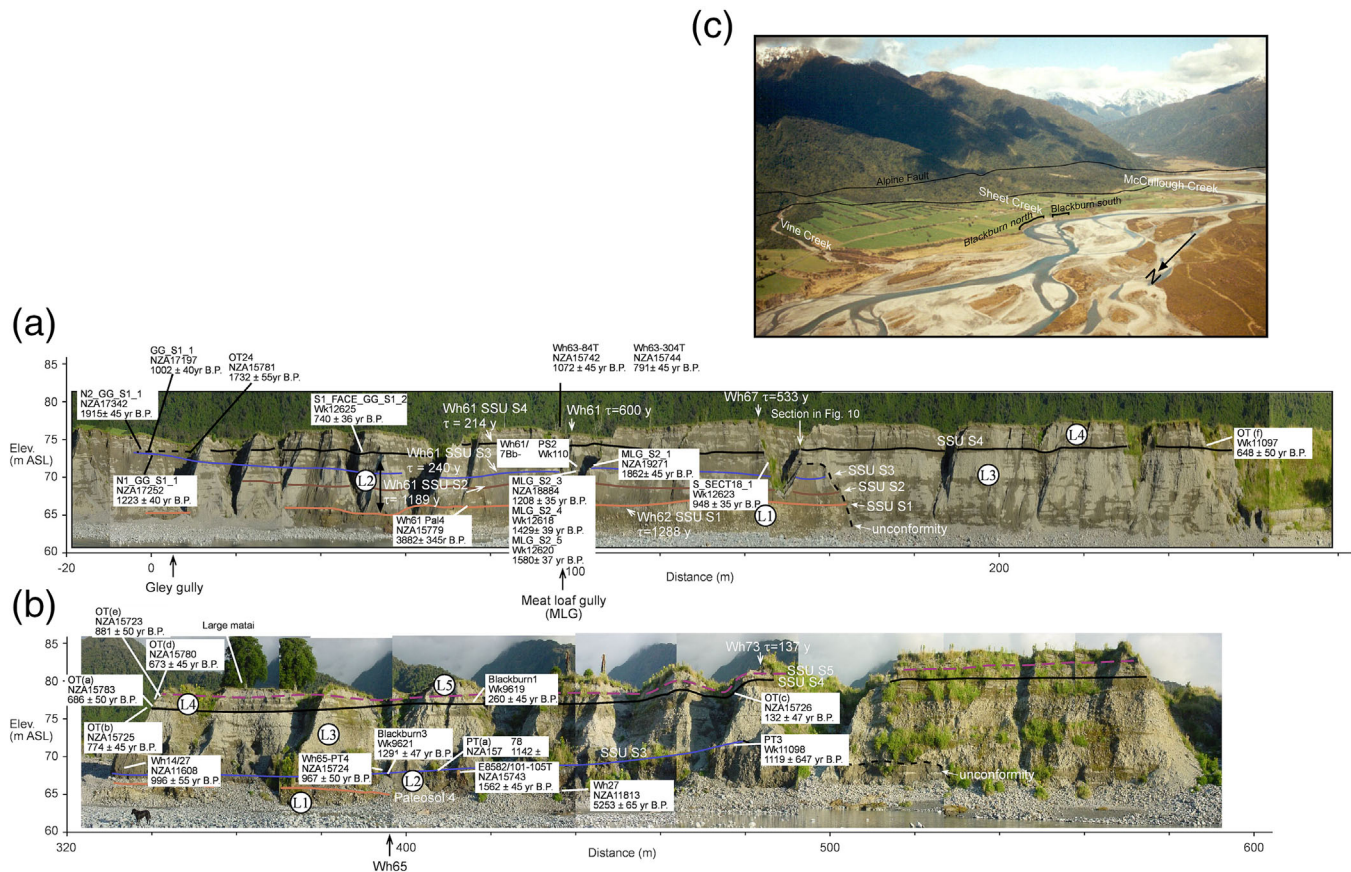
FIGURE 9 Blackburn exposure stratigraphy and radiocarbon ages along (a) the fan toe north of Sheet Creek and (b) the fan toe south of Sheet Creek. The nomenclature of sediment packages (L1, L2 etc.), soil stratigraphic units (S1 SSU, S2 SSU etc.) and soil residence times (SRTs) are discussed in the text and Table 1. Section locations and radiocarbon ages are listed in Table S1. The distance scale is metres southward from the start of exposure as shown in panel (c). Panel (c) locates the fan toe section on an oblique aerial photograph showing the incised state of the Whataroa River (photograph courtesy of Graham Hancox, GNS Science). The fan toe exposures are approximately 15–20 m high. The exposure shown in Figure 10 is indicated in panel (a) [Color figure can be viewed at wileyonlinelibrary.com]

overlapping dates of 3807–4245 and 2145–2463 BCE (Table S1). The PDI of an example of this SSU (Wh 62 at 110-m distance of the north section—Figure 9) calibrated to a residence time in the order of 1200 years. The directly overlying SSU in the north section, the S2 SSU, had no age control but similar SRT (Table 1).

The age control on the S3 SSU from the north section near Wh 61 (~100-m distance—Figure 9) came from wood, twigs, peat and other organic material (MLG_S2_3, MLG_S2_4, MLG_S2_5, Wh 61/7Bb_PS2 and Wh 61 Bc_PS2 in Table S1) that spanned the age range from 221 to 987 CE (Figure 11). This wide age range is inconsistent with the relatively short residence time (240 years) indicated by the example of this SSU we sampled at Wh 61 (Wh 61-PS2). Near the origin of the north section, the age range of the S3 SSU widened (S1_FACE_GG_S1_1, GG_S1_1, N1_GG_S1_1 and N2_GG_S1_1 in Table S1) to 35 BCE to 1281 CE and included an age characteristic of the overlying SSU (S4); we suspect that the SSUs in this area represent soils that form a composite (merged or 'welded', Morrison, 1998; Ruhe & Olson, 1980) profile as intervening fluvial sediments thin (to the north) and, thereby, host at least two populations of organic material. The S3 SSU in the south section yielded ages (PT3, PT (a), PT (b), Blackburn 3 in Table S1) that overlapped those of the S3 SSU on the north section but covered the narrower range of 675–1130 CE. A prone tree in the S3 SSU at 410 m along-section (E8582/101-105T in Table S1) with a ring count of 304 rings gave an age of 431–637 CE

from the 105th ring from the centre. Allowing for the offset, the outside of the tree had an age of 647–860 CE, which aligns it with the age of sample Blackburn 3 (twigs; 675–889 CE).

Three ages (S_SECT18_1, Wh 65-PT4 and Wh 14/27 in Table S1) from the thick alluvial fill burying the S3 SSU (sediment package L3) on the north and south sections ranged from 993 to 1214 CE, which overlapped the ages from the underlying SSUs but had a younger upper age limit concordant with the unit's position in the sequence. The S4 SSU sitting atop the alluvial fill was dated from the south and north sections including three ages from exposures along the true left of Sheet Creek gully (OT(a), (b), (d)–(f); S1_FACE_GG_S1 and 2 in Table S1), giving a relatively narrow range of ages from 1047 to 1419 CE. On the north section, the only age control above the S4 SSU came from the residence time of two surface soils (Wh 61 and Wh 67), which averaged 566 ± 17 years (SEM). Both soils were Immature Orthic Brown soils with ~10-cm-thick dark greyish brown A horizons over olive brown B horizons, which in the case of Wh 67 was composite in nature. On the south section, the S5 SSU interceded between the S4 SSU and the surface soil but there was no radiocarbon age control on that unit. The surface soil, based on profile Wh 73, had a residence time in the order of 200 years, consistent with later aggradation (burying the S5 SSU) than on the north section. The large living matai (*Prumnopitys taxifolia*) tree (Figure 10) growing
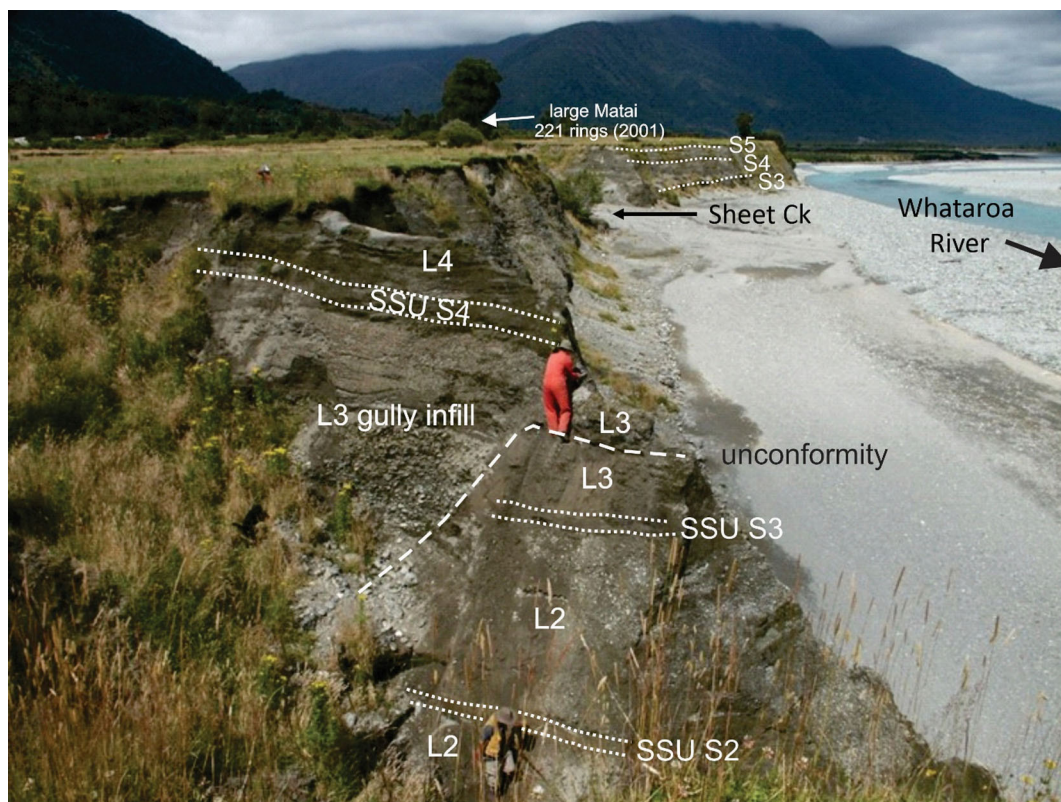
FIGURE 10 Photograph looking south over the Blackburn exposure with stratigraphy exposed in a small fan toe sapping gully north of Sheet Creek. The pronounced unconformity is the edge of an infilled gully cut through the fan sequence at 160 m in Figure 9. The position of soil stratigraphic units (SSUs) S2, S3 and S4 is indicated with intervening, ~2-m-thick fan aggradation units L2, L3 and L4 in the foreground. The matai tree-ring sample site at ~370 m along the south Blackburn toe face is in the distance. *Source*: Photograph courtesy of Gwendolyn Peters [Color figure can be viewed at wileyonlinelibrary.com]

on the south section had a ring count of 223 with an estimated 2 cm of wood missing to the core.

A final piece of age control came from a large standing but dead tree on the north section (Figure 9a; Wh 63 in Table S1). The tree was clearly buried part way up its trunk (Figure S6A). We felled the tree and dated two rings from a disc with 662 rings, one at the 84th ring from the centre (894–1154 CE) and the other from the 304th ring (1189–1385 CE). Modelling the sequence in OxCal gave times of establishment (allowing for the 23 ± 8-year lag for germination) and death of 865–1042 and 1553–1729 CE, respectively (Figure S6C). We dug at the tree's base and exposed a soil very similar to that at Wh 61 and Wh 67 described above (Figure S6B). At 2.17-m depth, we hit roots and a buried A horizon, possibly implying the tree established in the S4 SSU, which is buried at about that depth on the north section fan toe. However, when we tried to insert the tree establishment age in this stratigraphic position in the OxCal model, it produced poor agreement. We favour the interpretation that we uncovered a higher tier of roots that were the tree's response to an initial phase of burial and the tree instead established on sediment package L2, in the S3 SSU. Our interpretation implies that the tree is buried by as much as 5 m of fan sediment and our tree-ring-based ages may be significant under-estimates given that the time for the tree to reach about 6.5-m height is not accounted for. Nonetheless, even with an age under-estimation, the residence time of the S3 SSU accommodates the germination of the tree.

Our OxCal sequence model of the Blackburn stratigraphy (model agreement index 91.4%; Bronk Ramsey, 1995) does not include the old and conflicting ages associated with the S1 SSU, although they do

suggest an approximate date of 0–2 ky BCE (Table S1). The model indicates reasonable estimates for the timing of three aggradation events (Figure 11 and Table 2) corresponding to sediment packages L5, L4 and L3. The earliest dated aggradation (Event III—L3) backfilled a prior gully of Sheet Creek at 1030–1165 CE and overwhelmed the S3 SSU on the north and south sections. Radiocarbon ages from the S3 SSU on the north and south sections overlap, although, on the north section, the S3 SSU appears to have been forming for longer (longer residence time). On the south section, the S3 SSU had features characteristic of poor drainage in contrast to the well-drained nature of the S3 SSU on the north section. We interpret the differences in both soil character and SRT as arising from soils on a higher (north section) and a lower (south section) surface, the latter probably being an inset terrace. The base of the alluvial fill burying the S3 SSU geo-morphic surface lies below present river level, implying that incision extended deeper than the present gully before Event III aggradation (Figure 9). The aggradation overtopped the gully walls and deposited ~10 m of sandy gravel over the the S3 SSU on the south section and about 3.5 m over the S3 SSU on the north section to form an accor-dant surface on which the S4 SSU formed. This SSU was buried by about 2 m of sandy and fine gravelly alluvium during Event II (1335–1445 CE). On the south section, another phase of aggradation (Event I), most likely sourced from McCullough Creek, buried the contempo-rary surface soil, recognised as S5 SSU, at 1589–1768 CE (Figure 11 and Table 2). The behaviour of the fans at the Blackburn exposure over the last ca. 1 ka is summarised in Figure 8b.

Evidence of fan aggradation before Event III is preserved on the north section, corresponding to the southern flank of Vine Creek fan.
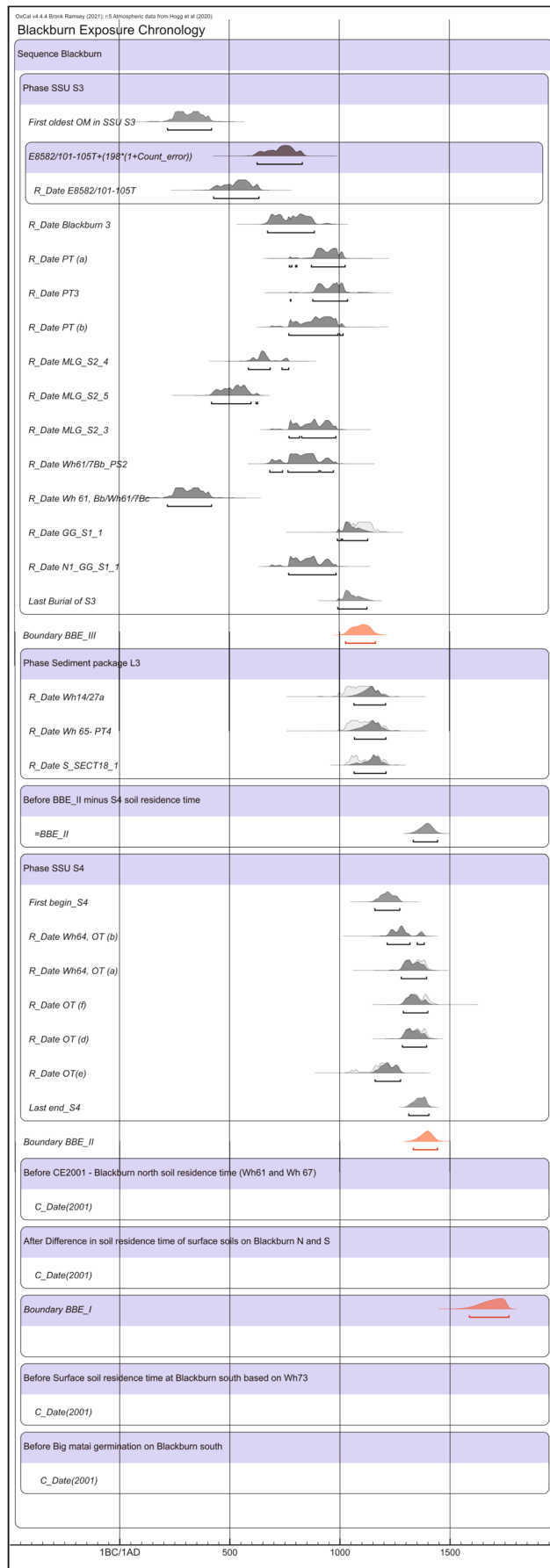
SSU S3 (Fig. S6 B) on the north section was a weakly expressed SSU (Weathered Fluvial Recent Soil, PDI = 1.4) showing only a 20 cm-thick olive-brown coloured Bw horizon. We infer that SSU S3 merges with SSU S4 (see below) to form a composite soil near the origin of the logged section. In the south section a peaty buried soil (Fig. S5 C) at about 67 m ASL was correlated to SSU S3 on the basis of radiocarbon ages. This SSU formed above an iron-stained cobble gravel we interpret as a lag gravel winnowed on the floor of an incising channel.

BBE_III burial of SSU S3
Sediment package L3 was a fining-up sequence of weakly imbricate, cobbly, sandy gravel that was coarser (including some boulders) on the south section and finer on the north section where it also included beds of loamy sediment. This sediment package lay adjacent and south of a steep angular unconformity at 160 m distance (Fig. 10) from which we infer it backfilled a prior gully then overwhelmed SSU S3 on first the south then the north sections to drape the whole fan toe exposure.

SSU S4 formed on the top of sediment package L3 and varied from a slightly peaty Gley Soil in the south section (Fig. S5 D) to a weakly developed Weathered Fluvial Recent Soil (Fig. S5 E) in the north section.

BBE_II burial of SSU S4
Sediment package L4 included sandy and loamy sediments with thin beds and pods of fine (channel fill) gravel up to 3 m thick. Its upper boundary formed the modern land surface on the north section but it was buried by another thin sediment package (L5 – see below) on the south section.
SSU S5 was a very weakly expressed upbuilding Recent Soil showing dark greyish brown, loamy cumulate A horizons in the top 1 m of sediment package L4. The cumulate A horizon included thin lenses (<10 cm) of fine gravel.
BBE_I burial of SSU S5 (south section only)
Sediment package L5 was found only on the south section where it was made up of about 1 m of loose, weakly imbricate, and dm-scale laminated fine gravelly coarse sand.
Surface soil
    South section- the surface soil formed in sediment package L5. The soil was a weakly developed Fluvial Recent Soil with no B horizon.
    North section - the surface soil formed into the older sediment package L4 and was an Immature Orthic Brown Soil (Fig. S5 F) with a 10 cm-thick dark greyish brown A horizon over a 20 cm-thick olive brown (2.5Y 4/3) Bw horizon

FIGURE 11 OxCal sequence model for the Blackburn exposure showing prior (light grey) and modelled (dark grey) calibrated 95% confidence interval probability density functions (PDFs) for radiocarbon ages. PDFs of boundaries between phases define aggradation event timings (red). Text provides summary lithological information. See the Supporting Information, Text ST2 for detailed stratigraphic information and Figure 9 for stratigraphy [Color figure can be viewed at wileyonlinelibrary.com]

Here, most of the sediment is sandy and fine gravelly, packages of sediment between SSUs are thin, and SSUs are well developed. This evidence suggests that the Vine Creek fan was relatively quiescent in the early to mid-late Holocene, depositing dominantly overbank sediment with only slowly accreting ground surfaces that allowed soils with multi-centennial to millennial residence times to form (SRT for S1 estimated at 1288 years) (Table 1).

3.3 | Other sites

Two other locations, one on the distal downstream toe of Little Man fan and the other on the middle of the piedmont reach of the Whataroa River, provided insights into the chronology of aggradation of the Whataroa River.

Site Wh 8 (Figures 2 and S7) exposed 6 m of fan-floodplain sediment with three intercalated buried soils at 2.5-, 3.5- and 6.0-m depth. We took woody material from a buried A horizon at 2.5-m depth, which returned a calibrated age of 1640 CE to present (Table S1). The soil was buried by sandy and loamy sediment with multiple rudimentary A horizons indicating incremental sediment accumulation, possibly coinciding with Event I or II on Little Man fan. The dated soil sat atop fine gravelly sands and silt lying over the second buried soil at 3.5 m, which we did not date. An auger boring below 3.5 m exposed loamy sands above another buried peat at 6-m depth. The peat gave a calibrated radiocarbon age of 685–998 CE (Table S1). This time period, when peat was accumulating at Wh 8, overlaps with the residence time of the S2 SSU at Little Man fan.

About midway (12 km) between the range front and the Tasman Sea at site Wh 13 (Figures 2 and S8), the Whataroa River exposed a stand of snapped trees in growth position in the river bed. We dated the outside of one tree to 778–1139 CE (Wh 13—Table S1), which overlaps with Event IV on Little Man and Event III on Blackburn exposure. A river bank section at Wh 13 revealed 3 m of silt with a single prominent but thin (10 cm) buried O horizon at 1.72-m depth, which we estimated to lie about 3 m above the dated riverbed tree. The silt burying this soil had multiple incipient A horizons indicating episodic rather than catastrophic accumulation. Shrub remains with broken stems were rooted in the horizon, from which wood (Wk8335) returned an age of 1502–1950 CE (Table S1), which may represent burial and death coeval with Event I or II from Little Man fan or Event I from the Blackburn exposure.

4 | DISCUSSION

Fans are relatively simple depositional systems because of direct links between sediment source areas and the depositional zone (Ventra & Nichols, 2014). However, their architecture and depositional history reflect both internal thresholds and feedbacks (autogenic effects) as well as external forcing (allogenic effects). The existence of both allogenic and autogenic forcing on fan dynamics means interpretations of fan stratigraphy need to be made with caution. In our study of the Te Taho fans, we are confident that allogenic effects, namely, earthquake-generated sediment pulses via landslides, dominate the depositional history. Our confidence stems from, first, the close correspondence of major aggradation events on fans from different catchments that have 200- to 300-year spacing, which is much longer than historic major storm event intervals. One in 100-year floods in Westland rivers are large (720–7462 m^3 s^{-1}), being almost twice the annual flood (Horrell et al., 2012), but we see no aggradation signal of the Te Taho fans at this timescale. Second, there is a close coincidence with known major earthquakes on the Alpine Fault (see Table 3 and discussion below). Autogenic responses in different fans are very unlikely to be coeval because they rely on subtle internal variations in the threshold of critical power related to changes in discharge, fan sediment reworking and channel gradient, amongst other effects. Additionally, aggradational responses on individual range front fans in Westland to landslides have been documented historically (Korup et al., 2004).

Two local, well-documented examples of single-catchment landslides are informative. In about 1918, the first records came to light (Griffiths & McSaveney, 1986) of rainfall and fluvial undercutting failures of the steep range front at Gaunt Creek (Figures 2 and 12)

TABLE 3 Time correlation between Te Taho fan aggradation events and large earthquakes on the central section of the Alpine Fault earthquakes.

Te Taho fan aggrad. onset	Timing[a] Little Man	Blackburn	AF; tab. S6 of Howarth et al. (2021) and Howarth et al. (2018)
1	1652–1800	1589–1768	1701–1732 *(co-called 1717 event) (S + C)*
2	1605–1669[b]		1549–1594 *(not AF)*
3	1318–1403	1335–1445	1384–1400 (S + C)
4	1041–1130	1030–1165	1148–1179 (S + C)
	Nil	Nil	*945–1010 (not AF)*
	Nil	Nil	936–978 (C)
5	425–888	Nil	396–626 (S + C?), 601–642 (C)
6	867 BCE to 169 CE	Nil	94–194 (S + C), 149–87 BCE (S + C), 387–330 BCE (S + C), 569–495 BCE (C), 854–789 BCE (S + C)

Abbreviations: C, central section; S, southern section.
[a]CE unless otherwise stated.
[b]92% confidence interval.

FIGURE 12 Photo mosaic (November 1969) showing location of Gaunt Creek landslide that initiated in ~1918 with fan building followed by incision on the Gaunt Creek and upper Waitangitoana fan and, in 1967, avulsion and building of the lower Waitangitoana fan downstream of State Highway (SH) 6 bridge and flow to Lake Wahapo. Residual drainage on the lower Waitangitoana fan feeds Graham Creek against the hillslope of Okarito Forest. Lidar-identified traces of Alpine Fault from Langridge et al. (2014). See Figure 2 for location. *Source*: Images from http://retrolens.nz and licensed by LINZ CC-BY 3.0 include run SN3208 images 4301 12 and 13, 4302 14 and 15, and 4303 15 and 16 [Color figure can be viewed at wileyonlinelibrary.com]
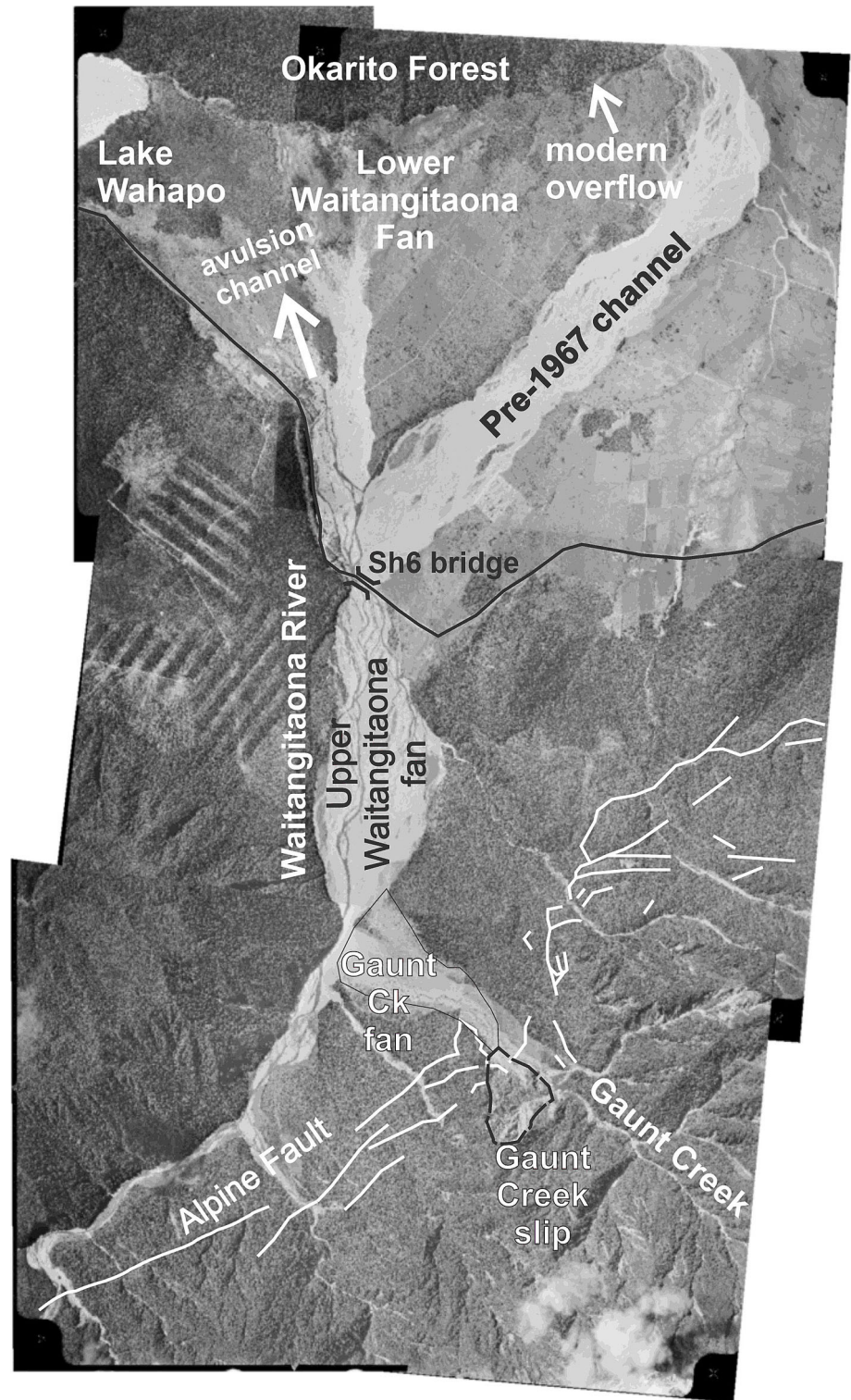
located in the fault-damaged zone of the Alpine Fault. Hamblett (1968) calculated a time-average input rate to the upper fan of 164 000 m^3 year^{-1} for the period 1918–1965, which infilled the fan channel and overwhelmed fluvial terraces in the upper catchment. From 1965 to 2001, the input rate of sediment reduced to 99 500 m^3 year^{-1} (Korup et al., 2004). The upper fan aggraded with at least 6 m of poorly sorted angular to subangular clast-supported pebble-cobble gravel with coarse sand matrix during the 1918–1965 period, followed by degradation of a similar amount after 1965 (Korup, 2005; Korup et al., 2004). The degradation of the upper fan post 1965 resulted in aggradation of at least 2 m on the lower fan

down to the State Highway (SH) 6 bridge and then progressively downstream on the Waitangitoana (Waitangitāhuna) River, resulting in avulsion of the river near Lake Wahapo in 1967 with prograding debris lobes invading farmland and swamp forest (Figure 12).

In 1999, a spontaneous failure from the flank of Mt Adams in the Poerua (Pouerua-tāhuna) catchment (Figure 2) with ~10 M m^3 of schist rock and colluvium (Hancox et al., 2005) provided further insight of a landslide and downstream aggradation. The landslide formed a 120-m-high dam, which blocked the Poerua River and impounded 5–7 M m^3 of water. The dam failed progressively over a 2-day period in a way that did not threaten lives, but subsequent

river aggradation (up to 20 m in gorges downstream of the landslide dam and about 4 m on the river downstream of the range front) and avulsion severely damaged pasture, fences and roads of a dairy farm in the upper part of the Poerua River fan (Korup et al., 2004). An attenuating wave of aggradation passed down the river reaching about 2 km from the range front over a 4-year period. The sediment discharge has been calculated as ~618 000 m³ a⁻¹, approximately 10 times the average Gaunt Creek landslide volume from 1918 to 2001. The river had begun to entrench at the fan apex adjacent to the range front by 2005 (Davies & Korup, 2007). More recent (2020–2022) lidar elevation data show that aggradation continued on the fan head to that time and extended about 3 km downstream from the fan apex (Figure S9). Hence, over the nearly two decades from 2005, the fan head aggraded (<1.5 m, see Figure S9) and pro-graded about 1 km, albeit influenced by river stopbanks (artificial levees) (see Beagley et al., 2020), which may have prevented avulsions.

The fan responses in the historical examples above have common elements: (1) Rapid delivery of sediment from the landslides causes channel aggradation at the fan head essentially immediately; (2) once the channel infills, aggradation and avulsion distribute sediment across the upper fan over multi-decadal timescales; and (3) after peak sediment delivery, the stream or river incises promptly at the fan head whereas aggradation and avulsion may occur lower on the fan as sediment is redistributed.

4.1 | Fan evolution

In Table 3, we correlate the ages of initiation of fan building at Te Taho with the most recent compilation of Alpine Fault (and Southern Alps) earthquakes (Howarth et al., 2021). Aggradation onsets 1, 3 and 4 (ca. 1717, 1400 and 1100 CE) overlap with Alpine Fault earthquake dates. Aggradation onset 2, at 1605–1669 CE (92% CI), postdates the non-Alpine Fault earthquake dated to 1549–1594 CE by Howarth et al. (2014) from lake sediments. These dates suggest that a delay of ca. 100 years between earthquake and aggradation cannot be ruled out, but we note that a peak in tree recruitment on the lower Whataroa floodplain at ca. 1650–1675 CE (Cullen et al., 2003) suggests that aggradation was waning or complete by then. If these trees established on deposits related to aggradation 2, then allowing for a decadal timescale for aggradation (Table 2 and modern examples), the onset of aggradation must have been close to the 1605 CE older age limit; hence, the delay between earthquake and aggradation may range from sub-decadal to ca. 50 years.

An absence of aggradation events corresponding to some Alpine Fault earthquakes (Table 3) indicates that the fan deposits described in our study are an incomplete record, which is not surprising given (1) the ~30% exposure we have available for study (Figure 4); (2) the proclivity of fan sedimentation to result in spatially discrete sediment packages corresponding to avulsion events (Field, 2001); and (3) repeated cut and fill especially along the fan axis. Our data show that at least the distributive components of sediment pulses are fre-quently stacked in a sequence enabling the analysis we have under-taken on the elapsed time for each phase of the fans' response. Thus, despite the record we document being incomplete, we believe it cap-tures the essence of range front fan response to earthquake-induced

sediment pulses. Moreover, the contrast in provenance of the allu-vium between the fans and the Whataroa River also allows us to infer aspects of the interaction of the small range front fans and the larger Whataroa River draining from the main divide of the Alps; and impor-tantly, we believe the system we study provides a model for much of the ~200 km of the central section of the Alpine Fault.

4.1.1 | The range front fan response cycle

Based on the consistent tempo of fan aggradation events and their coincidence with Alpine Fault or other earthquakes, we hypothesise a fan response cycle (FRC) linked to the earthquake cycle. We adopt the terminology of Bull (2008) to discuss phases of the FRC (Figure 13). An FRC begins with an earthquake, which perturbs the system by generating co- and post-seismic landslides (Fan et al., 2019), providing sediment for the fan.

Based on fault rupture length and displacement, Alpine Fault earthquakes have estimated magnitudes of Mw ≥ 7.5 for rupture of the central section and about Mw8 for multi-section rupture. These earthquakes generate shaking in the region of MM ≥ 9, resulting in widespread landsliding (Howarth et al., 2012; Robinson et al., 2016) of which, at least, 40%–60% (by volume) is likely to be directly con-nected to rivers (Li et al., 2016; Roback et al., 2018). Landslide sedi-ment delivered to a fan causes a reaction, whose lag from the triggering earthquake (the reaction time) we expect to be short given the high (>5 m) rainfall, short (3–6 km) steep gradients and historical analogues. In our chronology from the Te Taho fans (Table 3), aggra-dation and earthquake timings are mostly indistinguishable, and hence, the reaction time is too short for us to resolve. The two case studies of landslide-induced aggradation suggest sub-decadal reaction time, which we would not expect to resolve with radiocarbon. The style of initial reaction of the river is likely to include infilling of an incised channel at the fan head with the development of prograding fans on to the axial river floodplain at the trimmed fan toes (Leeder & Mack, 2001). The gravel we encountered in the range front fans was all schist derived, confirming that the initial aggradational response was to over-supply of sediment and not rising base level (i.e., aggrading axial river). Rising base level would have seen greywacke lithologies intercalated in the fan sediments (the 'axial allu-vium' of Leeder & Mack, 2001).

Relaxation time corresponds to the period of mining of landslide-generated sediment in the catchment and its transport onto the fan or beyond (Figure 13). We infer this involves backfilling of an incised stream channel then avulsion and sedimentation on the fan by dis-tributory lobes. On the Little Man fan, the exposure near the fan axis where the current river is incised shows cut-and-fill gravel packages. Away from the fan axis, sediment tended to be finer, consistent with distributory lobes and associated overbank sediment on a fan with no confined stream. Relaxation time represents the greatest instability on the broadest part of the fan surfaces, and therefore, in future, this will be when infrastructure and economic activity are most compromised.

Robinson and Davies (2013) estimate that a Mw8 earthquake on the Alpine Fault will generate in the order of 0.4–4 km³ of landslides over an area varying between 10⁴ and 10⁵ km², giving a characteristic yield of ~400 m³ ha⁻¹. If this yield were applied to the 15.7 km² Little Man catchment, then it would generate around 6 × 10⁵ m³ of eroded

(a)

Persistence time

Perturbation - Alpine Fault Earthquake

Sediment starvation, fan-head incision and down stream migrating intersection point, incision of main river and fan toe-cutting, driving entrenchment of fan stream and fan toe gullying. Metastable base-level.

Fan Response Cycle (FRC)

Reaction time 10^{-1} years

Landslide debris mobilisation and transport to the fan toe; landslide scar revegetation and soil stabilisation

Persistence time 10^2 - 10^3 years

Incision

Channel infilling followed by avulsion, distributive sedimentation, coeval aggradation of main river

Relaxation time 10^2 years

Legend

	Landslide
	Fan alluvium 2
	Fan alluvium 1
	River alluvium
	Fan deposition - bedload
	Fan deposition - overbank
	(Buried) geomorphic surface
	Fault rupture
	Bedrock

(b)

Streambed altitude

Reac-tion time | Relaxation time
Response time
Perist-ence time

Perturbation

alluvium

Time →

Stream at base level | Aggrad-ation | Incision | Stream at base level
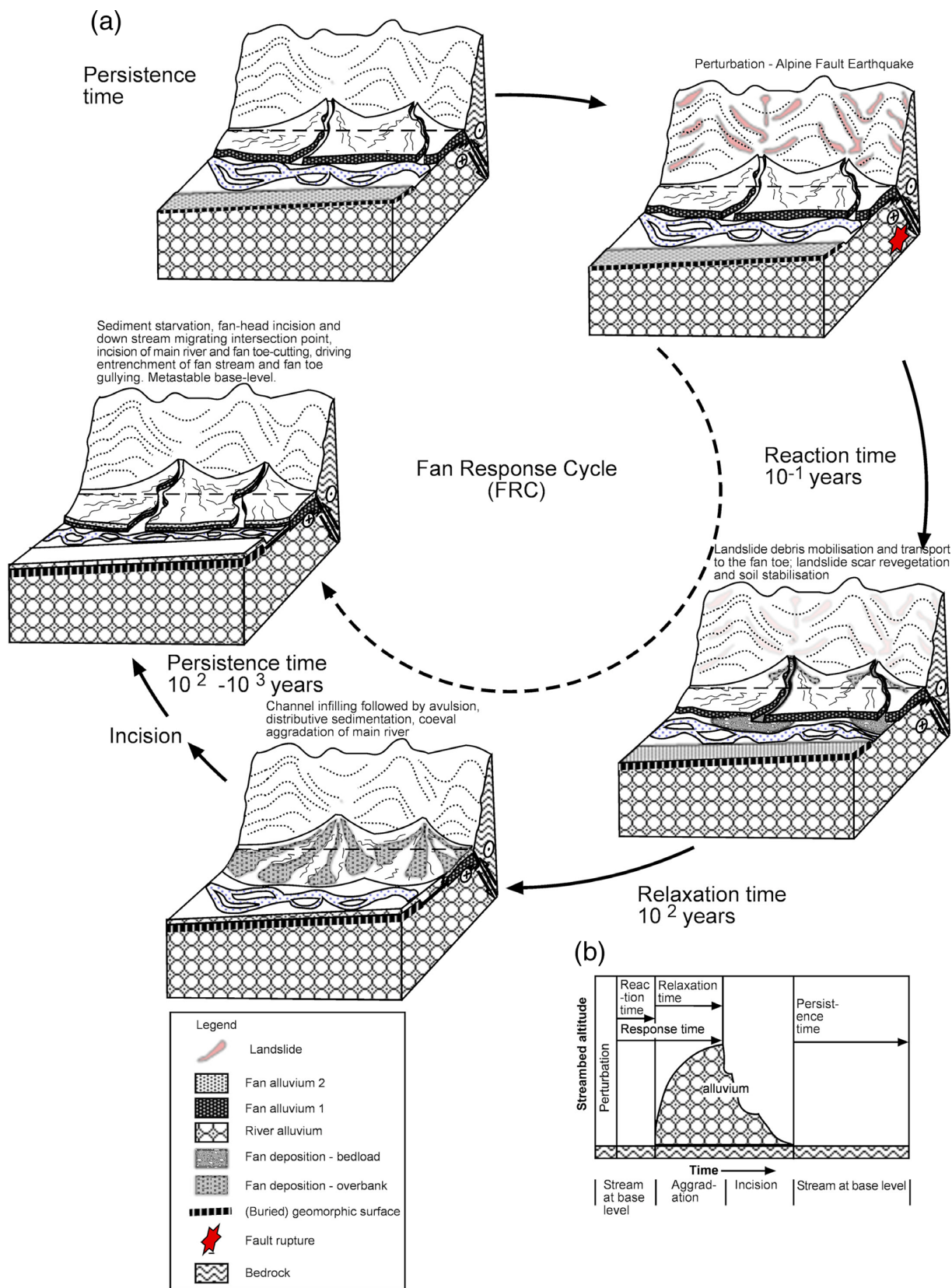
FIGURE 13 Process-response conceptual model for Alpine Fault earthquakes driving Te Taho fan evolution: (a) morphodynamic response showing timescales; and (b) definition of terminology (based on Bull, 2008). *Source*: The figure is reproduced with permission from John Wiley and Sons (#5371571339110): All rights reserved. No part of this panel may be reproduced, stored in a retrieval system or transmitted, in any form or by any means, electronic, mechanical, photocopying, recording or otherwise, except as permitted by the UK Copyright, Designs and Patents Act 1988, without the prior permission of the publisher [Color figure can be viewed at wileyonlinelibrary.com]

rock. Allowing for a factor of 2 decrease in the bulk density (increase in volume) of the failed rock, and no bypass of sediment to the axial river, the average amount of aggradation on the ~7 km² of fan would

be ~1.6 m. Although our fan toe section gives us a biased view of sedimentation on the whole fan, the estimate above appears to be too low given that we observed aggradation thicknesses in the order

of 2–4 m and assume no sediment bypass in the calculation. It is likely that the catchments of the range front fans generate disproportionately high yields compared with the region-wide average sediment yields proposed by Robinson and Davies (2013) because of their proximity to the fault, steeper than average slopes and weak cataclastic rocks. Our 95% CI estimates of the duration of the relaxation phase (duration of aggradation) range from effectively instantaneous to nearly two centuries based on OxCal models (Table 2). When sedimentation was distributive, minimum rates of aggradation were in the order of 10–15 mm year^{-1} for the three sediment packages associated with Little Man fan Events III, IV and V (ca. 1400 CE—L4; 1100 CE—L3; and 500 CE—L2). At the minimum rates, aggradation of 2–4 m would occur over a period of 130–400 years and would make economic use of the land difficult and costly. The localised aggradation following Event II (1650 CE) on Little Man fan between 900- and 1100-m distances along our measured section (Figure 5) appears to have been associated with an avulsion that deposited channel gravels in a broad lobe. Here, about 10 m of gravel accumulated over an inter-event interval of <129 years (Table 2), equating to a minimum aggradation rate of 80 mm year^{-1}. On Blackburn exposure, about 3 m of sediment package L4 accumulated after Event II and had a duration of 0–92 years, giving a minimum aggradation rate of 31 mm year^{-1}. These average rates obscure the likely punctuated and locally thick sedimentation that would make maintaining pasture and farm infrastructure impossible, as demonstrated by the Poerua River aggradation following the 1999 Mt Adams landslide (Davies & Korup, 2007).

Towards the end of the relaxation time, probably decades after initiating earthquakes, farming may once again become feasible, especially with some river control measures. SSUs and surface soils formed on aggradation packages often have cumulate B horizons, indicating that upbuilding pedogenesis (Almond & Tonkin, 1999) is common, whereby soil formation rates keep pace with sediment accumulation. Stream incision ends the period of relaxation whereupon the fan becomes dominantly stable, forest establishes broadly and soils shift from upbuilding to topdown pedogenesis (Almond & Tonkin, 1999) once the fan surface receives only rare and localised pulses of sediment.

The cycle ends with persistence time after the fan stream adjusts to lower sediment supply by incising, forming a lower gradient channel. During this phase, there is an approximate balance between sediment flux and the background catchment sediment yield. It is likely that, simultaneously, the axial river to which the fans grade has excess transport capacity and is capable of eroding sediment from its bed and margins, including the range front fan toes. Trimming enhances local base-level fall and ensures that most sediment bypasses the fan, leaving expansive fan surfaces stable for soil formation and forest re-establishment. Only the fan toes remain unstable where gullying and sapping erosion modify the scarps. This is the current condition of the Te Taho fans and Whataroa River fan.

Projecting forward to the likely response of the range front streams and fan sedimentation at Te Taho, an important consideration is the change in vegetation cover on the fans. Judging from areas in Westland unmodified by agriculture, the pre-European arrival events we see in the sedimentary record would have affected fans almost completely covered by forest. In contrast, there is almost no forest cover on the fans now. Therefore, the hydraulic roughness of the fan surfaces is markedly less and the character of aggradation is likely to

be different in future. We speculate that aggradation may take place in future via more discrete channelised deposition involving bedload and suspended load and less distributed deposition as in the past. Blagen et al. (2022) suggest that this effect may lead to less aggradation at fan heads and more towards fan toes, with a more rapid progression of aggradation down-fan.

Robinson and Davies (2013) noted that few alluvial fans are currently aggrading and that most fan heads are incised, as we see at the Te Taho fans. Therefore, most West Coast alluvial fans responding to Alpine Fault earthquakes are likely to have relatively short response times as Davies and Korup (2007) note, probably as a result of the frequent and large rainfall events (5000 mm year^{-1} at the range front and up to 12 000 mm year^{-1} near the crest of the Southern Alps) and steep river gradients. Howarth et al. (2012) were able to quantify the response time of landscape to Alpine Fault earthquakes from sediments accumulating in lakes adjacent to the Alpine Fault. They observed a threefold increase in sediment flux over a ~50-year period for each post-seismic landscape response.

A century-scale response time has been discussed in relation to the ~M8 1855 CE earthquake in the Remutaka Ranges of southern North Island (Hancox, 2005). There, the river bed prior to the earthquake had many bed-rock outcrops and rock pools, but in the aftermath of the earthquake aggradation of tens of metres occurred in the Orongorongo valley. However, Hancox noted that much of the landslide material remained on the hillslopes and a large storm in 2005 reactivated many of the landslides and led to a further pulse of aggradation. The rock strength in the Remutaka Range is comparable with the broken schist lithologies of the frontal hills of the Southern Alps but rainfall is much lower (~2.5 m a^{-1}) than on the West Coast.

Considerable analysis of post-earthquake effects has been undertaken following the Mw7.6 1999 Chi Chi earthquake in Taiwan and the M8 2008 Wenchuan earthquake in China (see Fan et al., 2019, for review). In Taiwan, much of the landslide material associated with the earthquake remains in the mountains east of the Chelengpu Fault and, after about 6 years, the initial sediment pulse had passed (Hovius et al., 2011). Hovius et al. (2011) and Yanites et al. (2010) also suggest that the seismically generated sediment in the Taiwan mountains may not be removed in the ~400-year repeat time of rupture on the Chelengpu Fault. Similarly, much of the landslide debris associated with the Wenchuan earthquake remains in place despite the massive and catastrophic landslides that did reach populated valley floor settings (Wang et al., 2017). Wang et al. (2017) suggest that it will be years to decades for the sedimentation rate to decay to pre-earthquake levels in the Longmenshan Range.

Although there are many similar characteristics between landslides and sediment transfer in the Te Taho fans and historic international events, there are marked differences in some of the key drivers of fan building particularly related to river power. River power in West Coast rivers and streams is substantially greater than in Taiwan where maximum rainfall is about 4000–5000 and ~1000 mm year^{-1} in the Longmenshan Range of China (Gao et al., 2016). So, in both locations, annual rainfall is lower than the West Coast setting and, additionally, the West Coast rivers and streams have at least twice the gradient of catchments affected by the Chi Chi and Wenchuan earthquakes (Croissant et al., 2017). Thus, our assessment that the Te Taho range front fans respond very rapidly to earthquake forcing and have the

ability to transport the debris quickly and efficiently to the piedmont is consistent with international observations, but we suggest that they may represent an extreme of sediment transport efficiency and response time (see fig. 4 of Croissant et al., 2017).

4.1.2 | Behaviour of the axial (Whataroa) river

Implicit in our conceptual model of the behaviour of range front fans, there is an upstream ('topdown', Mather et al., 2017) control on fan aggradation. Thus, range front fans may aggrade asynchronously with the axial river, and the magnitude and timing of aggradation may not directly reflect what is happening on the larger axial river fan. In contrast, we contend that incision on the range front fans is tightly coupled with axial river behaviour. Deep entrenchment of fan toes cannot occur without a base-level fall ('bottom up control', Mather et al., 2017). Therefore, the episodes of incision we document on the Te Taho fans most probably correspond to incision and lateral erosion by the Whataroa River. We discuss periods of axial river incision first and then consider its aggradation.

Currently, the Whataroa River is incised into its fan and is trimming the toes of the Te Taho range front fans, which represents the persistence time of the most recent FRC (i.e., FRC 1, which started in 1717 CE). At the Alpine Fault, the Whataroa River is entrenched more than 10 m below the fan head (see fig. 4 of Langridge et al., 2018) and streams flowing across the Te Taho fans are deeply incised. Langridge et al. (2018) estimated the timing of incision of the Whataroa River at the range front after the most recent aggradation to 1706–1823 CE. From the residence time of soils and the large matai tree on Blackburn south section, we estimate that the most recent incision on the fan was complete by 1730–1749 CE whereas incision on the Little Man fan was complete by 1696–1866 CE. The close correspondence is consistent with our contention that there is tight coupling between Te Taho fans and the Whataroa River during incision phases.

Based on stratigraphic relations between SSUs and sediment packages, we have evidence for incision on Little Man fan before FRC 2 and FRC 4, which began about 1600 and 1100 CE, respectively (Figure 8). At the Blackburn exposure, there is evidence of incision before FRC 3, which began ca. 1100 CE. Elsewhere, a radiocarbon age (Rafter ID 40706/6) from wood recovered from a drill hole at the Deep Fault Drilling Programme (DFDP) site 2B (Figure 3) at the Alpine Fault indicates that, at 1277–1388 CE, the Whataroa River was incised at least 20 m below the present river bed (Thomas, 2018). This site is only 4 km upstream from the Blackburn exposure, so it seems likely that incision on that fan would have occurred, albeit not in the interfan zone we logged. Its timing corresponds to the end of FRC 3 at Blackburn. In summary, (1) many of the FRCs including the current one are characterised by periods when channels are incised on one or both fans; and (2) our chronology suggests that these phases dominate the response cycle of both the range front fans and the Whataroa River. In other words, most of the 'work' (of aggradation and incision) is completed in a small part of the whole cycle leaving long periods (10^2–10^3 years; see Figure 13) when fans are relatively stable with forest growth and soil development.

The synchronicity or otherwise of aggradation of the range front fans and the axial river can only be addressed empirically. The statistically indistinguishable ages of the exhumed trees at Wh 13, 12 km down the Whataroa fan, and Te Taho Event IV (1100 CE) cannot resolve any lag time between aggradation on the range front fans and the Whataroa fan. Five kilometres upriver from the Alpine Fault (Figure 2), Blagen (2021) determined the colonisation of forest on a terrace 15 m above the river by tree ring counting. The earliest colonisation was estimated to be 1425 CE. Assuming that the terrace is aggradational, the 1400 CE event had culminated before 1425 CE and must postdate the age from 20-m depth in the DFDP-2B core described above. An OxCal model of the sequence (Table S3) constrains the aggradation event and duration of aggradation in the alpine reach of the river to 1293–1433 CE and 34–170 years, respectively. These ranges are indistinguishable from those of Te Taho aggradation 3 (Tables 2 and 3), meaning if there is any lag in response or difference in tempo of aggradation between the range front fans and the Whataroa River, it is undetectable by our means. As discussed above, a histogram of tree colonisation dates from the lower Whataroa fan (Cullen et al., 2003) suggests that a pulse of aggradation was complete before 1650 CE and another by 1725 CE. These dates of culmination of aggradation are consistent with the Whataroa fan aggrading coeval with the Te Taho fans (see aggradation onsets 2 and 1, respectively, Table 3). In summary, and with reference to the discussion above, we have no reason to believe the range front fans and the Whataroa fan do not aggrade or incise in-step. Thus, we feel confident that the range front fans are a reliable proxy for behaviour of the Whataroa fan whose behaviour presents the greatest hazard locally (Blagen et al., 2022).

4.2 | Implications for hazard and risk

Our data on the history and evolution of the Te Taho fans provide high-resolution information on likely future hazard and risk when the Alpine Fault next ruptures in the anticipated M8 earthquake. Most of the findings confirm the basis for prior hazard and risk assessments (Blagen et al., 2022; McDonald et al., 2018; Orchiston, 2013; Orchiston et al., 2018; Robinson & Davies, 2013; Westland District Council, 2006).

From our data, the relaxation time of the Te Taho fans (basically the aggradation phase) is estimated to range from years to decades but <200 years (Table 2), in keeping with historic events in New Zealand and international literature. Many studies infer an initial decadal reaction time (Croissant et al., 2017). In the initial relaxation phase, one can imagine that the Te Taho fan location would be too unpredictable for safe or effective occupation with stream avulsion, continued high rates of aggradation especially at times of large rainfall events or aftershocks. The economic and psychosocial effects if farming of the fans was attempted are likely to be profound. Alongside the immediate impacts of aggradation on pasture productivity, animals and farm infrastructure, and seismically induced damage to infrastructure (shaking, liquefaction and landslide damage) (Westland District Council, 2006), up to a decade of aftershocks would add to the stress burden. Our data also suggest that the larger area of the Whataroa floodplain would experience disastrous disturbances with similar timing and tempo. Our results show (Figure S8C) that as much as 5 m of sediment ranging from silt to fine gravel has accumulated 12 km down-valley from the range front in the last ca. 1000 years. This result corroborates findings from tree ages and

confirms that most of the Whataroa fan will experience protracted aggradation that threatens livelihoods, exacerbating the acute hazard of flooding of an aggrading river. Later in the relaxation phase, it may be possible, with active management of stream courses, excavation of sediment from channels and warning systems for the transport route and farming to resume.

The singularity and fragility of SH 6 is well known even under non-earthquake conditions (Gorman, 2019; Westland District Council, 2006). Our data from Whataroa provide an indication of the likely outage time at this locality and some insight into what is likely to occur along a significant proportion of the highway between Hokitika in the north and Haast Pass in the south (Figure 1) where SH 6 is both the single highway connecting the region and within 30 km of the Alpine Fault. The distance between these locations is 337 km and, for ~130 km, the road either crosses alluvial floodplains or range front alluvial fans prone to inundation exemplified by the Whataroa study site. For a further ~130 km, the road crosses steep, unstable terrain prone to rockfall and debris flow inundation triggered by strong ground shaking (Zorn et al., 2018). The road crosses the Alpine Fault at several locations including bridges crossing the Wanganui, Whataroa, Waiho, Fox, Cook and Karangarua Rivers along a 90-km length of central Westland. Major damage if not collapse of these bridges and their approaches is anticipated when the expected 6–10 m of surface displacement occurs in future earthquakes, and other bridges are prone to shaking-induced collapse (Westland District Council, 2006). As noted above, at individual locations, road transport along the West Coast connecting isolated farming and tourism communities can be expected to be cut for months to years and this will be exacerbated by bridge damage or destruction. The compounding consequences of the number of locations where road and bridge repairs will be necessary, coupled with the difficulty in getting machinery into remote locations, will necessitate working outward from a limited number of 'bridgeheads' where plant, machinery and fuel are available to begin repair work. Reopening SH 6 is likely to take many years (Blagen et al., 2022) even after alluvial sedimentation in floodplains and range front fans has diminished.

5 | CONCLUSIONS

Our study of the range front fans at Te Taho on the north side of the Whataroa River has involved mapping and dating exposures of multi-episode fans at the fan toe where they have been trimmed by the incised and laterally migrating Whataroa River. Complementary exposures were provided by local streams graded to the larger Little Man River or Whataroa River, and sapping gullies eroding back from the trimmed toe locations. The sequences exposed on the Little Man fan and Blackburn exposure are similar for the past several cycles but differ in detail of aggradation deposits and depth of stream incision. Comparing FRCs with the timing of known Alpine Fault earthquakes confirms that initial aggradation is very likely to be earthquake triggered. However, not all fan building episodes are exposed in our study and, thus, our sequence is incomplete, with bypassing of fan aggradation in successive events a likely cause. Nevertheless, we have identified and dated four major episodes of fan building since 1000 CE. Sixty-two radiocarbon ages, SRTs and stratigraphic ordering have been used as input to OxCal sequence models for the Little Man fan

(30 ages) and Blackburn exposure (19 ages) (Figures 7 and 11) that constrain event times to 1041–1130, 1318–1445, 1605–1754 and 1652–1800 CE. SRTs quantify the duration of periods when rates of aggradation were minimal or nil and hence have allowed us to constrain the duration of rapid aggradation (Table 2 and Figure 8). In many cases, the SRT values are very similar to the inter-event intervals, confining the period of rapid aggradation to narrow time windows. Although there are significant uncertainties in determining event timing from radiocarbon dating and in the determination of SRT, the conclusion is that the time taken for the accumulation of fan alluvium is short compared with inter-event time and the periods of relative stability when soils formed and mature forest developed on the fans. The germination date and time of death of several *in situ* trees rooted in various soil horizons in the fans have also been established from radiocarbon dating of closely constrained ring numbers in the trees (Figure S3). These data confirm the efficacy of the SRT methodology. Therefore, we are confident that range front fan behaviour is dominantly controlled by pulses of sediment generated by infrequent major events spaced at ~100- to 300-year intervals.

The age model of the fans links well with the most recent determination of Alpine Fault earthquakes (and other events considered to be Southern Alps events; Howarth et al., 2021) (Table 3 and Figure 8), and we consider it very likely that there will be a substantial response to all major Alpine Fault and Southern Alps earthquakes in these and other similar fans.

We show that fans and axial rivers respond in-step with almost immediate reaction to landsliding, followed by rapid aggradation followed quickly by incision at the fan head and along the steep stream channels and main floodplain. Total response time (including reaction, relaxation and incision phases of the FRC; Figure 13) is <2 centuries and possibly as short as multi-decadal. Where fan surfaces have stabilised, we have determined SRTs of up to ~240 years for successive events, but where fan surfaces are not overwhelmed in successive events, then SRTs of >1000 years have been calculated.

Our data on the evolution of the Te Taho fans are consistent with other historic non-earthquake events on the West Coast but faster than other earthquake sites in New Zealand and internationally where rainfall and elevation gradients (the basis for stream power) are lower.

Judging from the thickness of fan deposits exposed in the fan toe areas of the Te Taho fans and the short duration of aggradation (Table 2), we conclude that current farming practices on the fans and probably across much of the Whataroa River fan are most unlikely to be sustainable for a decade to several decades after a major earthquake. We partly base this conclusion on observations from non-earthquake, localised landslides that occurred in range front catchments at Gaunt Creek and Poerua River. The recovery after aggradation, including re-establishment of farm infrastructure and productive pasture, represents a further delay, which remains poorly quantified. The sustainability of current land-use practices, regional tourism and agriculture are at risk, more so because of reliance on infrastructure including the highly vulnerable single arterial highway (SH 6; see Westland District Council, 2006).

ACKNOWLEDGEMENTS

DATA AVAILABILITY STATEMENT

The data that support the findings of this study are available from the corresponding author upon reasonable request.

ORCID

Peter C. Almond https://orcid.org/0000-0003-4203-1529

REFERENCES

Abrams, M.J. & Chadwick, O.H. (1994) Tectonic and climatic implications of alluvial fan sequences along the Batinah coast, Oman. *Journal of the Geological Society*, 151(1), 51–58. Available from: https://doi.org/10.1144/gsjgs.151.1.0051

Almond, P.C. & Tonkin, P.J. (1999) Pedogenesis by upbuilding in an extreme leaching and weathering environment, and slow loess accretion, south Westland, New Zealand. *Geoderma*, 92(1-2), 1–36. Available from: https://doi.org/10.1016/S0016-7061(99)00016-6

Assine, M.L., Corradini, F.A., do Nascimento Pupim, F. & MM, M.G. (2014) Channel arrangements and depositional styles in the São Lourenço fluvial megafan, Brazilian Pantanal wetland. *Sedimentary Geology*, 301, 172–184. Available from: https://doi.org/10.1016/j.sedgeo.2013.11.007

Beagley, R., Davies, T. & Eaton, B. (2020) Past, present and future behaviour of the Waiho River, Westland, New Zealand: a new perspective. *Journal of Hydrology. New Zealand*, 59(1), 41–61.

Berryman, K., Cooper, A., Norris, R., Villamor, P., Sutherland, R., Wright, T. et al. (2012) Late Holocene rupture history of the Alpine fault in South Westland, New Zealand. *Bulletin of the Seismological Society of America*, 102(2), 620–638. Available from: https://doi.org/10.1785/0120110177

Blagen, J.R. (2021) *A dendrogeomorpholgical study of aggradation hazards in Westland, New Zealand*. University of Canterbury,Christchurch, New Zealand, p. 279.

Blagen, J.R., Davies, T.R.H., Wells, A. & Norton, D.A. (2022) Post-seismic aggradation history of the West Coast, South Island, Aotearoa/New Zealand; dendrogeomorphological evidence and disaster recovery implications. *Natural Hazards*, 114(3), 2545–2570.

Blair, T.C. & McPherson, J.G. (2009) Processes and forms of alluvial fans. In: *Geomorphology of desert environments*. Springer, Dordrecht, pp. 413–467 https://doi.org/10.1007/978-1-4020-5719-9_14

Bronk Ramsey, C. (1995) Radiocarbon calibration and analysis of stratigraphy: the OxCal program. *Radiocarbon*, 37(2), 425–430. Available from: https://doi.org/10.1017/S0033822200030903

Bronk Ramsey, C. (2009) Bayesian analysis of radiocarbon dates. *Radiocarbon*, 51(1), 337–360. Available from: https://doi.org/10.1017/S0033822200033865

Bull, W.B. (1977) The alluvial-fan environment. *Progress in Physical Geography*, 1(2), 222–270. Available from: https://doi.org/10.1177/030913337700100202

Bull, W.B. (2008) *Tectonic geomorphology of mountains: a new approach to paleoseismology*. Blackwell Publishing,Oxford, U.K.

Cochran, U.A., Clark, K.J., Howarth, J.D., Biasi, G.P., Langridge, R.M., Villamor, P. et al. (2017) A plate boundary earthquake record from a wetland adjacent to the Alpine fault in New Zealand refines hazard estimates. *Earth and Planetary Science Letters*, 464, 175–188. Available from: https://doi.org/10.1016/j.epsl.2017.02.026

Cox, S.C. & Barrell, D.J.A. (2008) *Geology of the Aoraki area: scale 1: 250000*. GNS Science, Lower Hutt, New Zealand.

Croissant, T., Lague, D., Steer, P. & Davy, P. (2017) Rapid post-seismic landslide evacuation boosted by dynamic river width. *Nature Geoscience*, 10(9), 680–684. Available from: https://doi.org/10.1038/ngeo3005

Cullen, L.E., Duncan, R.P., Wells, A. & Stewart, G.H. (2003) Floodplain and regional scale variation in earthquake effects on forests, Westland, New Zealand. *Journal of the Royal Society of New Zealand*, 33(4), 693–701. Available from: https://doi.org/10.1080/03014223.2003.9517753

Dade, W.B. & Verdeyen, M.E. (2007) Tectonic and climatic controls of alluvial-fan size and source-catchment relief. *Journal of the Geological Society*, 164(2), 353–358. Available from: https://doi.org/10.1144/0016-76492006-039

Davey, F.J. (2010) Crustal seismic reflection profile across the Alpine Fault and coastal plain at Whataroa, South Island. *New Zealand Journal of Geology and Geophysics*, 53(4), 359–368. Available from: https://doi.org/10.1080/00288306.2010.526545

Davies, T.R.H. & Korup, O. (2007) Persistent alluvial fanhead trenching resulting from large, infrequent sediment inputs. *Earth Surface Processes and Landforms*, 32(5), 725–742. Available from: https://doi.org/10.1002/esp.1410

DeCelles, P.G. & Cavazza, W. (1999) A comparison of fluvial megafans in the Cordilleran (Upper Cretaceous) and modern Himalayan foreland basin systems. *Geological Society of America Bulletin*, 111, 1315–1334.

DeMets, C., Gordon, R.G. & Argus, D.F. (2010) Geologically current plate motions. *Geophysical Journal International*, 181(1), 1–80. Available from: https://doi.org/10.1111/j.1365-246X.2009.04491.x

Eger, A., Almond, P.C. & Condron, L.M. (2011) Pedogenesis, soil mass balance, phosphorus dynamics and vegetation communities across a Holocene soil chronosequence in a super-humid climate, South Westland, New Zealand. *Geoderma*, 163(3-4), 185–196. Available from: https://doi.org/10.1016/j.geoderma.2011.04.007

Fan, X., Scaringi, G., Korup, O., West, A.J., van Westen, C.J., Tanyas, H. et al. (2019) Earthquake-induced chains of geologic hazards: patterns, mechanisms, and impacts. *Reviews of Geophysics*, 57(2), 421–503. Available from: https://doi.org/10.1029/2018RG000626

Field, J. (2001) Channel avulsion on alluvial fans in southern Arizona. *Geomorphology*, 37(1-2), 93–104. Available from: https://doi.org/10.1016/S0169-555X(00)00064-7

Gao, M., Zeilinger, G., Xu, X., Tan, X., Wang, Q. & Hao, M. (2016) Active tectonics evaluation from geomorphic indices for the central and the southern Longmenshan range on the Eastern Tibetan Plateau, China. *Tectonics*, 35(8), 1812–1826. Available from: https://doi.org/10.1002/2015TC004080

Gorman, P. (2019) *Questions over future of West Coast's SH6 if Alpine Fault quake hits*. Available from: https://www.stuff.co.nz/national/111891615/questions-over-future-of-west-coasts-sh6-if-alpine-fault-quake-hits. (Accessed: 15/4/2022)

Griffiths, G.A. (1979) High sediment yields from major rivers of the western Southern Alps, New Zealand. *Nature*, 282(5734), 61–63. Available from: https://doi.org/10.1038/282061a0

Griffiths, G.A. & McSaveney, M.J. (1983) Distribution of mean annual precipitation across some steepland regions of New Zealand. *New Zealand Journal of Science*, 26, 197–209.

Griffiths, G.A. & McSaveney, M.J. (1986) Sedimentation and river containment on Waitangitaona alluvial fan-South Westland, New Zealand. *Zeitschrift für Geomorphologie*, 30(2), 215–230. Available from: https://doi.org/10.1127/zfg/30/1986/215

Hamblett, S. (1968) *Waitangi-taona River report*. Christchurch: Water and Soil Division, Ministry of Works and Development.

Hancox, G.T. (2005) Landslides and liquefaction effects caused by the 1855 Wairarapa earthquake: then and now. In: *The 1855 Wairarapa earthquake symposium*. Greater Wellington Regional Council Wellington, Wellington, New Zealand.

Hancox, G.T., McSaveney, M.J., Manville, V.R. & Davies, T.R. (2005) The October 1999 Mt Adams rock avalanche and subsequent landslide dam-break flood and effects in Poerua river, Westland,

New Zealand. *New Zealand Journal of Geology and Geophysics*, 48(4), 683–705. Available from: https://doi.org/10.1080/00288306.2005.9515141

Harvey, A.M. (2002) Effective timescales of coupling within fluvial systems. *Geomorphology*, 44(3-4), 175–201. Available from: https://doi.org/10.1016/S0169-555X(01)00174-X

Hicks, D.M., Shankar, U., McKerchar, A.I., Basher, L., Lynn, I., Page, M. et al. (2011) Suspended sediment yields from New Zealand rivers. *Journal of Hydrology. New Zealand*, 50, 81–142.

Hogg, A.G., Heaton, T.J., Hua, Q., Palmer, J.G., Turney, C.S.M., Southon, J. et al. (2020) SHCal20 Southern Hemisphere calibration, 0–55,000 years cal BP. *Radiocarbon*, 62(4), 759–778. Available from: https://doi.org/10.1017/RDC.2020.59

Horrell, G.A., McKerchar, A.M., Griffiths, G.M. & Griffiths, G.A. (2012) South Island storms and floods of December 2010. *Journal of Hydrology. New Zealand*, 51, 63–81.

Hovius, N., Meunier, P., Lin, C.-W., Chen, H., Chen, Y.-G., Dadson, S. et al. (2011) Prolonged seismically induced erosion and the mass balance of a large earthquake. *Earth and Planetary Science Letters*, 304(3-4), 347–355. Available from: https://doi.org/10.1016/j.epsl.2011.02.005

Hovius, N., Stark, C.P. & Allen, P.A. (1997) Sediment flux from a mountain belt derived by landslide mapping. *Geology*, 25(3), 231–234. Available from: https://doi.org/10.1130/0091-7613(1997)025<0231:SFFAMB>2.3.CO;2

Howarth, J.D., Barth, N.C., Fitzsimons, S.J., Richards-Dinger, K., Clark, K.J., Biasi, G.P. et al. (2021) Spatiotemporal clustering of great earthquakes on a transform fault controlled by geometry. *Nature Geoscience*, 14(5), 314–320. Available from: https://doi.org/10.1038/s41561-021-00721-4

Howarth, J.D., Cochran, U.A., Langridge, R.M., Clark, K., Fitzsimons, S.J., Berryman, K. et al. (2018) Past large earthquakes on the Alpine Fault: paleoseismological progress and future directions. *New Zealand Journal of Geology and Geophysics*, 61(3), 309–328. Available from: https://doi.org/10.1080/00288306.2018.1464658

Howarth, J.D., Fitzsimons, S.J., Norris, R.J. & Jacobsen, G.E. (2012) Lake sediments record cycles of sediment flux driven by large earthquakes on the Alpine fault, New Zealand. *Geology*, 40(12), 1091–1094. Available from: https://doi.org/10.1130/G33486.1

Howarth, J.D., Fitzsimons, S.J., Norris, R.J. & Jacobsen, G.E. (2014) Lake sediments record high intensity shaking that provides insight into the location and rupture length of large earthquakes on the Alpine Fault, New Zealand. *Earth and Planetary Science Letters*, 403, 340–351. Available from: https://doi.org/10.1016/j.epsl.2014.07.008

Howarth, J.D., Fitzsimons, S.J., Norris, R.J., Langridge, R. & Vandergoes, M. J. (2016) A 2000 yr rupture history for the Alpine fault derived from Lake Ellery, South Island, New Zealand. *Bulletin of the Geological Society of America*, 128(3–4), 627–643. https://doi.org/10.1130/b31300.1

Keefer, D.K. (1999) Earthquake-induced landslides and their effects on alluvial fans. *Journal of Sedimentary Research*, 69(1), 84–104. Available from: https://doi.org/10.2110/jsr.69.84

Korup, O. (2005) Geomorphic imprint of landslides on alpine river systems, southwest New Zealand. *Earth Surface Processes and Landforms*, 30(7), 783–800. Available from: https://doi.org/10.1002/esp.1171

Korup, O., McSaveney, M.J. & Davies, T.R. (2004) Sediment generation and delivery from large historic landslides in the Southern Alps, New Zealand. *Geomorphology*, 61(1-2), 189-207.

Langridge, R.M., Howarth, J.D., Cox, S.C., Palmer, J.G. & Sutherland, R. (2018) Frontal fault location and most recent earthquake timing for the Alpine Fault at Whataroa, Westland, New Zealand. *New Zealand Journal of Geology and Geophysics*, 61(3), 329–340. Available from: https://doi.org/10.1080/00288306.2018.1509878

Langridge, R.M., Ries, W.F., Farrier, T., Barth, N.C., Khajavi, N. & De Pascale, G.P. (2014) Developing sub 5-m LiDAR DEMs for forested sections of the Alpine and Hope faults, South Island, New Zealand: implications for structural interpretations. *Journal of Structural Geology*, 64, 53–66. Available from: https://doi.org/10.1016/j.jsg.2013.11.007

Langridge, R.M., Villamor, P., Howarth, J.D., Ries, W.F., Clark, K.J. & Litchfield, N.J. (2021) Reconciling an early nineteenth-century rupture of the Alpine fault at a section end, Toaroha River, Westland, New Zealand. *Bulletin of the Seismological Society of America*, 111(1), 514–540. Available from: https://doi.org/10.1785/0120200116

Larsen, I.J., Almond, P.C., Eger, A., Stone, J.O., Montgomery, D.R. & Malcolm, B. (2014) Rapid soil production and weathering in the Southern Alps, New Zealand. *Science*, 343(6171), 637–640. Available from: https://doi.org/10.1126/science.1244908

Leeder, M.R. & Mack, G.H. (2001) Lateral erosion ('toe-cutting') of alluvial fans by axial rivers: implications for basin analysis and architecture. *Journal of the Geological Society*, 158(6), 885–893. Available from: https://doi.org/10.1144/0016-760000-198

Li, G., West, A.J., Densmore, A.L., Hammond, D.E., Jin, Z., Zhang, F. et al. (2016) Connectivity of earthquake-triggered landslides with the fluvial network: implications for landslide sediment transport after the 2008 Wenchuan earthquake. *Journal of Geophysical Research - Earth Surface*, 121(4), 703–724. Available from: https://doi.org/10.1002/2015JF003718

Mather, A.E., Stokes, M. & Whitfield, E. (2017) River terraces and alluvial fans: the case for an integrated Quaternary fluvial archive. *Quaternary Science Reviews*, 166, 74–90. Available from: https://doi.org/10.1016/j.quascirev.2016.09.022

McDonald, G.W., Smith, N.J., Kim, J.-H., Brown, C., Buxton, R. & Seville, E. (2018) Economic systems modelling of infrastructure interdependencies for an Alpine Fault earthquake in New Zealand. *Civil Engineering and Environmental Systems*, 35(1-4), 57–80. Available from: https://doi.org/10.1080/10286608.2018.1544627

McKeague, J.A. & Day, J.H. (1966) Dithionite- and oxalate-extractable Fe and Al as aids in differentiating various classes of soils. *Canadian Journal of Soil Science*, 46(1), 13–22. Available from: https://doi.org/10.4141/cjss66-003

Milne, J.D.G., Clayden, B., Singleton, P.L. & Wilson, A.D. (1995) *Soil description handbook*. Lincoln, Canterbury: Manaaki Whenua Press.

Morrison, R.B. (1998) How can the treatment of pedostratigraphic units in the North American stratigraphic code be improved? *Quaternary International*, 51-52, 30–33. Available from: https://doi.org/10.1016/S1040-6182(98)90197-5

Mouchené, M., van der Beek, P., Carretier, S. & Mouthereau, F. (2017) Autogenic versus allogenic controls on the evolution of a coupled fluvial megafan–mountainous catchment system: numerical modelling and comparison with the Lannemezan megafan system (northern Pyrenees, France). *Earth Surface Dynamics*, 5(1), 125–143. Available from: https://doi.org/10.5194/esurf-5-125-2017

North American Commission on Stratigraphic Nomenclature. (2005) North American stratigraphic code. *American Association of Petroleum Geologists Bulletin*, 89, 1547–1591.

Orchiston, C. (2013) Tourism business preparedness, resilience and disaster planning in a region of high seismic risk: the case of the Southern Alps, New Zealand. *Current Issues in Tourism*, 16(5), 477–494. Available from: https://doi.org/10.1080/13683500.2012.741115

Orchiston, C., Mitchell, J., Wilson, T., Langridge, R., Davies, T., Bradley, B. et al. (2018) Project AF8: developing a coordinated, multi-agency response plan for a future great Alpine Fault earthquake. *New Zealand Journal of Geology and Geophysics*, 61(3), 389–402. Available from: https://doi.org/10.1080/00288306.2018.1455716

Roback, K., Clark, M.K., West, A.J., Zekkos, D., Li, G., Gallen, S.F. et al. (2018) The size, distribution, and mobility of landslides caused by the 2015 Mw7.8 Gorkha earthquake, Nepal. *Geomorphology*, 301, 121–138. Available from: https://doi.org/10.1016/j.geomorph.2017.01.030

Robinson, T.R. & Davies, T.R.H. (2013) Potential geomorphic consequences of a future great ($M_w = 8.0+$) Alpine Fault earthquake, South Island, New Zealand. *Natural Hazards and Earth System Sciences*, 13(9), 2279–2299. Available from: https://doi.org/10.5194/nhess-13-2279-2013

Robinson, T.R., Davies, T.R.H., Wilson, T.M. & Orchiston, C. (2016) Coseismic landsliding estimates for an Alpine Fault earthquake and the consequences for erosion of the Southern Alps, New Zealand. *Geomorphology*, 263, 71–86. Available from: https://doi.org/10.1016/j.geomorph.2016.03.033

Ruhe, R.V. & Olson, C.G. (1980) Soil welding. *Soil Science*, 130(3), 132–139. Available from: https://doi.org/10.1097/00010694-198009000-00004

Schlunegger, F. & Norton, K.P. (2015) Climate vs. tectonics: the competing roles of Late Oligocene warming and Alpine orogenesis in constructing alluvial megafan sequences in the North Alpine foreland basin. *Basin Research*, 27(2), 230–245. Available from: https://doi.org/10.1111/bre.12070

Schoeneberger, P.J., Wysocki, D.A., Benham, E.C. & Staff, S.S. (2012) *Field book for describing and sampling soils, Version 3*. Lincoln, Nebraska, USA: Natural Resources Conservation Service, USDA: National Soil Survey Centre.

Sibson, R.H., White, S.H. & Atkinson, B.K. (1981) Structure and distribution of fault rocks in the Alpine Fault Zone, New Zealand. *Geological Society Special Publication*, 9, 197–210.

Thomas, A.M. (2018) *Glacio-lacustrine sedimentation in newly discovered paleo-lakes, Westland, New Zealand*. Master's Thesis, Te Herenga Waka—Victoria University of Wellington, Wellington, New Zealand, p. 158.

Tonkin, P.J. & Basher, L.R. (1990) Soil stratigraphic techniques in the study of soil and landform evolution across the Southern Alps, New Zealand. *Geomorphology*, 3(3-4), 547–575. Available from: https://doi.org/10.1016/0169-555X(90)90020-Q

Ventra, D. & Nichols, G.J. (2014) Autogenic dynamics of alluvial fans in endorheic basins: outcrop examples and stratigraphic significance. *Sedimentology*, 61(3), 767–791. Available from: https://doi.org/10.1111/sed.12077

Wang, W., Godard, V., Liu-Zeng, J., Scherler, D., Xu, C., Zhang, J. et al. (2017) Perturbation of fluvial sediment fluxes following the 2008 Wenchuan earthquake. *Earth Surface Processes and Landforms*, 42(15), 2611–2622. Available from: https://doi.org/10.1002/esp.4210

Wells, A. & Goff, J. (2006) Coastal dune ridge systems as chronological markers of palaeoseismic activity: a 650-yr record from southwest New Zealand. *The Holocene*, 16(4), 543–550. Available from: https://doi.org/10.1191/0959683606hl949rp

Wells, A. & Goff, J. (2007) Coastal dunes in Westland, New Zealand, provide a record of paleoseismic activity on the Alpine fault. *Geology*, 35(8), 731–734. Available from: https://doi.org/10.1130/G23554A.1

Wells, A., Yetton, M.D., Duncan, R.P. & Stewart, G.H. (1999) Prehistoric dates of the most recent Alpine Fault earthquakes, New Zealand. *Geology*, 27(11), 995–998. Available from: https://doi.org/10.1130/0091-7613(1999)027<0995:PDOTMR>2.3.CO;2

Westland District Council. (2006) *Westland District Council lifelines study: Alpine Fault earthquake scenario & lifelines vulnerability assessment*. Westland District Council, Hokitika, New Zealand, p. 210.

Yanites, B.J., Tucker, G.E., Mueller, K.J. & Chen, Y.-G. (2010) How rivers react to large earthquakes: evidence from central Taiwan. *Geology*, 38(7), 639–642. Available from: https://doi.org/10.1130/G30883.1

Yoo, K. & Mudd, S.M. (2008) Discrepancy between mineral residence time and soil age: implications for the interpretation of chemical weathering rates. *Geology*, 36(1), 35–38. Available from: https://doi.org/10.1130/G24285A.1

Zorn, C., Davies, A., Robinson, T., Pant, R., Wotherspoon, L. & Thacker, S. (2018) Infrastructure failure propagations and recovery strategies from an Alpine Fault earthquake scenario. In: *Proceedings of the 16th European Conference on Earthquake Engineering, Thessaloniki, Greece*. European Association for Earthquake Engineering (EAEE), Turkey, pp. 18–21.

SUPPORTING INFORMATION

Additional supporting information can be found online in the Supporting Information section at the end of this article.